Title: Single-Nucleus Transcriptomics Reveals How Cell Type Shapes the Circadian Transcriptome of the Arabidopsis Leaf

Alveena Zulfiqar[1,2], Zachary A. Myers[1,2], Ananda Menon[1], and Kathleen Greenham[1]

[1] Department of Plant and Microbial Biology, University of Minnesota, St. Paul, MN 55108, USA

[2] These authors contributed equally to this work.

Author for correspondence:

Kathleen Greenham
Plant and Microbial Biology
1479 Gortner Ave 140 Gortner Lab
St Paul MN 55108
812-360-1483
greenham@umn.edu

Keywords: single-nuclei, transcriptome, gene regulatory network, circadian clock, Arabidopsis

Abstract

Circadian regulation enables plants to coordinate cellular processes with daily environmental cycles, yet the dynamics and hierarchy of the clock across cell types remains poorly understood. To characterize circadian regulation across cell types in the mature *Arabidopsis thaliana* leaf, we performed a 24 hour single nucleus RNA-sequencing circadian time course. We captured ~30,000 nuclei across seven circadian time points, recovering all major leaf cell types. We identified over 7,400 genes with cluster-resolved circadian regulation, and used coexpression analysis to define five major temporal expression clades shared across all cell types. We leveraged these assignments to identify genes with cell-type-specific temporal shifts in expression. Single cell gene regulatory networks were generated for each cluster through GENIE3, identifying many shared and unique transcription factor target interactions across clusters. A close examination of core clock component targets identified complex light and hormone signaling associated networks, capturing both broad cross-cell type regulation and cell-type-specific target regulation. Our results demonstrate the extent to which circadian transcriptional regulation is present in the mature Arabidopsis leaf, and highlight the immense complexity in cell-type-specific regulation.

52 **Background**

53 The Earth's rotation on its axis generates predictable fluctuations in the day-night cycle.
54 Organisms from unicellular to complex multicellular species, including humans, have evolved
55 endogenous circadian oscillators (1). These autonomous time-keeping mechanisms allow
56 organisms to anticipate and adapt to the dramatic yet predictable daily changes in light and
57 temperature that arise from the day-night cycle that is a consequence of the Earth's rotation on its
58 axis (1, 2). The circadian mediated alignment of cellular processes with external cues is central to
59 survival and fitness (3). Although clock genes vary across kingdoms, the fundamental principles
60 of circadian regulation, such as transcriptional-translational feedback loops and entrainment by
61 environmental cues known as zeitgebers, are remarkably conserved (4–8).

62

63 In plants, the circadian clock is integral to coordinating physiological processes with daily
64 environmental changes, ensuring optimal growth, metabolism and development (9–11). The plant
65 circadian system consists of transcriptional regulators that function through transcriptional-
66 translational feedback loops to generate rhythmic gene expression patterns with a roughly 24-hour
67 period (12, 13). Dawn expressed *CIRCADIAN CLOCK ASSOCIATED 1* (*CCA1*) and *LATE*
68 *ELONGATED HYPOCOTYL* (*LHY*) MYB transcription factors (TFs) are followed by the
69 sequential expression of the transcriptional repressors *PSEUDO RESPONSE REGULATORS*
70 *PRR9, PRR7*, *PRR5,* and *PRR3,* and the evening-phased *TIMING OF CAB EXPRESSION 1*
71 *(TOC1)/PRR1* (14–19). Additional repressors include the Evening Complex (EC), consisting of
72 *LUX ARRHYTHMO (LUX), EARLY FLOWERING 3 (ELF3)* and *ELF4* that contribute to circadian
73 clock function and coordinating growth and development (20). *NIGHT LIGHT-INDUCIBLE AND*
74 *CLOCK-REGULATED1 (LNK1)* and *LNK2* act as co-activators of *REVEILLE4* (*RVE4*) and *RVE8*

to positively regulate *PRR5, TOC1* and the EC (19, 21–23). *LIGHT-REGULATED WD1* (*LWD1*) and *LWD2* are additional co-activators that along with *TEOSINTE BRANCHED 1-CYCLOIDEA-PCF20* (*TCP20)* and *TCP22* positively regulate *CCA1*, *PRR9,* and *PRR7 (24, 25)*. These regulatory arrangements facilitate robust circadian gene expression across environmental variation, and allow the clock to gate and influence target genes across time and cell types.

Unlike the centralized circadian control observed in mammals, where the suprachiasmatic nucleus acts as the master pacemaker (26), plants possess a decentralized network of circadian oscillators distributed across tissues and organs therefore creating a complex system to understand the interplay between local clocks (27). Across certain cell types there is evidence to suggest a complex hierarchical organization of circadian oscillators in plants. The shoot apical meristem (SAM) appears to serve as a dominant clock (28), providing long distance signaling to the root clock (29); however, detached roots can maintain rhythmicity (30), suggesting the SAM is not required for sustained clock function. Cell-type-specific circadian clocks have been shown to regulate distinct physiological processes, supporting the importance of local coupling of oscillators within a cell type. For example, the vascular clock plays a pivotal role in controlling flowering time via regulation of *FLOWERING LOCUS T (FT)* expression in phloem companion cells (31–33), while epidermal clocks modulate temperature-dependent cell elongation (32). Local signaling provides additional synchronization as observed in the leaf, where the vascular clock appears dominant over the mesophyll clock (31).

Several studies have shown that different plant organs and cell types maintain distinct circadian periods (27, 31, 34–38). In Arabidopsis seedlings, the cotyledon and hypocotyl have been found

98 to exhibit shorter periods than the root (27, 35, 37), whereas guard cells exhibited longer periods
99 compared to adjacent mesophyll and epidermal cells (39), and vascular cells maintained more
100 robust circadian rhythms compared to mesophyll cells (31, 35). Regions of high cell density, such
101 as shoot and root meristems, tend to have more tightly coupled clocks, whereas the leaf can
102 maintain independent phases of circadian clock gene promoter oscillations across itself (28, 36,
103 38). Single cell imaging of a pCCA1::CCA1-YFP fusion protein and bioluminescence recording
104 of a LUCIFERASE (LUC) reporter driven by the promoter for the clock component *GIGANTEA*
105 (*GI::LUC)* at near cellular level revealed cell-type-specific differences, such as the shorter periods
106 observed in root tips compared to other regions across the root (27, 37). These cell-type-variations
107 in clock behavior highlight the complexity of intra-tissue clock partitioning and emphasize the
108 need to understand the importance of these distinct oscillators.
109
110 Traditionally, the study of plant circadian rhythms has been limited to methods such as bulk RNA
111 sequencing (RNA-seq) and microarray based mRNA capture, both of which mask cell-type-
112 specific nuances by averaging signals across heterogeneous cell populations. Recent technological
113 advances, including single-cell and single-nucleus RNA-sequencing, have enabled unprecedented
114 resolution and provided an opportunity to unravel cell specific circadian regulation (40–42). A
115 snRNA-seq circadian time course on 8-day old Arabidopsis seedlings revealed highly conserved
116 rhythmic expression of the core clock genes across most cell types, yet their phase and amplitude
117 was highly variable. Consistent with cell-type-specific roles of the circadian clock, most circadian
118 regulated genes were identified in single clusters. Cotyledons exhibited more pronounced intra
119 tissue cycling gene similarity than the root, although phase differences were observed across
120 subclusters suggesting altered clock characteristics even within a cell type (43, 44). A

121 comprehensive understanding of how these cell-type-specific oscillators regulate distinct
122 biological processes over the continued development of the plant will facilitate more targeted
123 approaches for improving plant growth.
124
125 In this study, we captured the transcriptional profiles of over 30,000 nuclei across a 24 hour
126 circadian time course to investigate circadian regulation in mature leaves of Arabidopsis. This
127 high-resolution analysis revealed the existence of distinct circadian oscillators operating within
128 specific cell types and enabled us to identify five predominant phase dependent expression clades
129 present across all cell types. Through a single cell gene regulatory network analysis we resolved
130 cluster specific and conserved regulatory connections across cell types. Our findings provide new
131 insights into the intricate, decentralized nature of plant circadian clocks and will contribute as a
132 comprehensive resource for future research to understand tissue specific clock architecture.
133
134 **Results**
135 **Construction and cell type identification of a circadian single nucleus time course in mature**
136 **leaves of Arabidopsis**
137 To capture circadian clock regulated genes across different cell types in the Arabidopsis leaf, we
138 conducted a single nucleus RNA sequencing (snRNA-seq) time course experiment on 13 day old
139 Arabidopsis plants. We entrained seedlings to a 12 hour photoperiod at 22°C for 11 days prior to
140 transfer to constant light (LL) (Fig. 1A). Pairs of samples were collected over 24 hours at four-
141 hour intervals starting at ZT48 (zeitgeber, hours after dawn), isolating above-ground tissue by
142 cutting over the root:shoot junction. Fresh tissue was immediately used for nuclei isolation and
143 10X Genomics-based single nuclei capture. Initial assessment of these libraries through Cellranger

144 (45) revealed promising nuclei capture rates ranging from ~2,000-4,000 for most libraries, and
145 median genes detected metrics were similar to several previously reported single nucleus libraries
146 in plants, ranging from ~1,000-1,500 genes detected (Table S1) (41, 44, 46). We observed higher
147 than expected levels of background RNA (as defined by the fraction of reads assigned to cells in
148 Cellranger), likely due to our sampling decision to minimize handling time by skipping both
149 fluorescence activated nuclei sorting and density gradient purification, and note that of the initial
150 14 snRNA-seq libraries, one library did not pass QC (ZT24B), and one library had reduced nuclei
151 capture rates (Table S1) (ZT04B).
152
153 Previous single cell circadian studies in Arabidopsis and mouse systems found that unguided
154 integration of time course datasets can lead to phase-specific clustering, where genes with peak
155 expression at a certain time of day influence clustering and obfuscate cell-type-specific signatures
156 (44, 47). Core clock components, such as *CCA1*, are widely expressed across cell types (27). We
157 reasoned that our experimental design might introduce phase-specific biases not captured in single
158 time point single cell experiments. We observed that a large portion of cluster specific cell-type-
159 markers identified in previous experiments have been shown to be circadian regulated (Fig. 1B),
160 with a handful of cell types defined by a majority of genes previously observed to cycle (48, 49).
161 We found that we could achieve cell-type-specific clustering by masking ~7,000 circadian
162 regulated genes from integration anchoring, and subsequently using a large set of 15,000 variable
163 genes as integration anchors (Fig. 1C). To construct our circadian gene list, we combined the full
164 set of cycling genes previously identified through bulk RNA-seq (48), and merged this list with
165 genes identified as cycling in our own pseudo-bulk data (see methods). Our time course captured
166 ~30,000 high quality nuclei, with predicted identities from all the major tissue types found in the

167 Arabidopsis leaf. A majority of the nuclei captured were identified as actively photosynthetic or
168 of mesophyll origin, with relatively smaller numbers of well described cell types, such as guard
169 cells, phloem companion cells, and dividing cells (Fig. 1D). This includes many cell types with a
170 high proportion of circadian regulated marker genes, such as guard cells, which were often missing
171 or unresolved when integrated without masking.
172
173 Tissue and cell-type-assignments were confirmed by examining expression of previously reported
174 marker genes (Table S2), and further refined by Gene Ontology (GO) enrichment analyses and
175 cluster-specific biomarker analysis (Fig. 1E-H, Table S3). Cluster-specific expression of
176 previously reported marker genes identified Clusters 6, 9 and 14 as phloem companion cells,
177 dividing cells, and guard cells, respectively (Fig. 1E). Examining the most significantly enriched
178 GO terms in each cluster highlighted tissue of origin very effectively for mesophyll, epidermal,
179 and photosynthetic cells, with GO terms associated with water use, fatty acid biosynthesis, and
180 light harvesting among the most enriched terms for each cell type (Fig. 1F, Table S1). Finally, we
181 used cluster-specific biomarkers to refine our cell-type-assignments in many clusters (Fig. S1).
182 Expression of *FAMA*, a bHLH transcription factor involved in stomatal development (50), was
183 highly specific to Cluster 14, with moderate expression only found in Cluster 13 (Fig. 1G).
184 Expression of *NPCC6* (*NUCLEAR-ENRICHED PHLOEM COMPANION CELL GENE 6*) was
185 previously reported to be highly specific to phloem companion cells (51), and was identified as a
186 highly significant Cluster 6 biomarker in our dataset (Fig. 1H). Together our detailed analytical
187 approach of leveraging marker gene expression, GO enrichment analysis and cluster-specific
188 biomarkers has successfully identified all major leaf cell types in our snRNA-seq circadian time
189 course.

190

191 **Cycling gene expression is widespread across all cell types of the mature Arabidopsis leaf**

192 To explore circadian regulation in our dataset, we examined pseudo-bulk expression profiles of
193 circadian clock components and outputs over our single nucleus time course (Fig. 2A). We saw
194 robust oscillations coinciding with previously reported expression patterns in all of the examined
195 components (48, 52, 53). We next examined whether these expression patterns persisted within
196 and across clusters for a suite of circadian clock components (Fig. 2B, S2). We observed similar
197 expression patterns across most clusters for *CCA1* and *TOC1*, showing robust and similar cycling
198 across a large number of clusters. In contrast, many clock components were only identified as
199 cycling in a subset of clusters. In most cases, such as with *GI, LUX*, and *PRR5*, patterns were
200 consistent across clusters in which they were called cycling; however, a handful of clock
201 components were observed with shifted phase in one or more clusters. One striking example of
202 this is *ELF3*, which has an earlier phase in guard cells (Fig. 2B). In order to better characterize
203 these expression patterns, we utilized JTKcycle (54) to identify cycling genes using both pseudo-
204 bulk and cluster-resolved expression values with p adj < 0.05. We identified 4,769 genes with
205 cycling gene expression patterns in our pseudo-bulked dataset (Table S4). Our analysis revealed
206 that ~68% (3264/4769) of our rhythmic genes from the pseudo-bulk data set overlap with a
207 previous bulk-RNAseq circadian regulated gene list (48).

208

209 Cluster-specific cycling genes were identified for all clusters other than Cluster 16, where tissue
210 sampling variability likely drove non-uniform distribution of root hair cell type across the time
211 course (Fig. S3). The total number of genes identified with cluster-specific cycling patterns ranged
212 from ~1,800 in Cluster 0, to ~300 in Cluster 8_1 (Fig. 2D, Table S5). While we noted that the

213 clusters with the fewest identified cycling genes were also relatively small clusters, our ability to
214 consistently capture robust rhythms for key clock TFs such as CCA1 and TOC1 was encouraging
215 (Fig. 2B). We observed 4,825 genes cycling within at least one cluster, and noted that more than
216 half of all cycling genes were identified as cycling in only a single cluster (Fig. 2E). Examination
217 of the phase of cycling markers in each cluster identified that most clusters contain genes with
218 peak expression across our time course; however, a handful of clusters have clear biases towards
219 cycling genes at key time periods, including an apparent over-representation of morning-phased
220 cycling genes in guard cells (Fig. S4). Many core clock components were identified as cycling in
221 many clusters, with *CCA1* and *TOC1* significantly cycling in 18 and 14 clusters across the dataset
222 respectively, and found that the shifted expression observed in *ELF3* in guard cells met our
223 threshold for significance (Fig. 2B). Due to our decision to process nuclei from fresh tissue at
224 every time point, a 48-h time course was not feasible. To limit the false-negatives associated with
225 capturing a single cycle we included a biological replicate at every time point to help reduce this
226 concern, and have adopted a stringent significance threshold for cycling status (55). As a
227 consequence of this, we are confident that genes that exceed our cutoffs are truly cycling; however,
228 we refrain from making strong claims about the set of non-cycling genes without examining
229 individual gene expression patterns.
230
231 Our analysis revealed 7,417 rhythmic genes across clusters with 59% overlapping with previous
232 bulk RNA-seq data (Fig. S5) (48). Furthermore, we observed a significant overlap of cycling genes
233 between our data set and a recent 24 h and 48 h circadian snRNA-seq data set (44), with 41% of
234 genes identified as cycling genes in the 24 h dataset and 63% overlapping with the 48 h dataset
235 (Fig. S5). The high overlap with the 48 h time course supports our inclusion of a second replicate

236 and indicates that we have identified a significant number of genes that have been previously
237 reported as circadian regulated at bulk and at the single cell level.
238
239 **Coexpression network analysis identifies five major temporal expression patterns across all**
240 **cell types**
241 Due to the limitations inherent in calling phase from a single 24 hour cycle (54) we confirmed the
242 cycling and phase using the weighted gene correlation network analysis (WGCNA) package in R
243 (56). The method has been previously applied for grouping cycling genes with similar phases into
244 modules (57, 58). This resulted in clustering of genes based on expression pattern into 26 modules.
245 To remove genes with weak correlations with the module eigengene pattern, we filtered the
246 modules by kME (Module Eigengene connectivity) value; only genes with kME $\geq$ 0.6 were
247 retained. We next calculated correlation metrics for the modules identified by using the average
248 zScore of each module for the time course. We then used the metrics to perform hierarchical
249 clustering of the modules. Euclidean distance calculated from the correlation values, where shorter
250 distance indicates strong relationship and more similarity between the modules, identified five
251 major clades among all modules. Representative expression patterns for each clade was calculated
252 by averaging the zScore of all the genes and resulted in five major gene expression patterns
253 throughout the day: early morning (clade 3), morning (clade 2), mid day (clade 1), evening (clade
254 4) and late night (clade 5) phased genes (Fig. 3A, Table S6). Additionally, we examined the
255 distribution of the five clades across our clusters and each cell type had representation of all five
256 expression patterns (Fig. 3B). Some cell types were more enriched in certain expression patterns,
257 for example C5 (Vasculature) and C14 (GC) clusters had a larger proportion of genes with morning
258 expression pattern (clade 2).

To analyze the biological processes enriched for the clades identified, we performed GO enrichment analysis (Table S3). The GO analysis identified some common and unique enrichment terms among the clades; the early morning clade (clade 3) had genes involved in auxin response, tropism and regulation of stomatal closure. Similarly, we saw enrichment of genes for indole-containing compound catabolic/biosynthesis processes and cellular response to ABA enriched in the midday clade (clade 2). The GO terms related to preparation for photosynthetic machinery were enriched in the second half of the day indicating the plant's strategy to prepare for the energy harvesting processes of the next day (Fig. 3A).

To examine whether genes cycling across clusters exhibited similar phase patterns we identified genes that were found in multiple clades. The majority of genes (5611) were exclusive to one clade only, whereas 1540, 114, and 1 gene were found in 2, 3, and 4 clades respectively. For the genes present in two clades, we find most shifts occurred between adjacent clades (Fig. 3C; grey ribbons); however, a small fraction of genes exhibited more dramatic phase changes (Fig. 3C; yellow ribbons). Examining these genes at the cluster level revealed similar changes between clusters suggesting a common regulatory mechanism (Fig. 3D). Notably, we identified a handful of genes in our photosynthesizing cluster that showed phase changes when compared to phloem companion cell (PCC) or guard cell (GC), resulting in their segregation into different clades (Fig. 3D). As our analysis revealed that the same genes can have cell-type-specific expression patterns, we next aimed to construct cell-type-specific gene regulatory networks to enhance our understanding of the unique regulatory mechanism at play in each cell type.

282 **Single cell gene regulatory networks uncover cell-type-specific circadian regulation of gene**
283 **expression**

284 We next constructed circadian single cell gene regulatory networks (scGRNs) to better
285 characterize the ways in which circadian genes are differentially regulated across tissues. We
286 implemented the GENIE3 algorithm on individual clusters while simultaneously limiting our input
287 dataset to genes which were cycling in that specific cluster. In parallel, we iteratively shuffled each
288 cluster's data and ran GENIE3 to identify null distributions of each dataset. The weight value
289 corresponding to the 95th percentile was used as a weight cutoff for the unshuffled connections,
290 leaving ~156,000 TF-target connections spread across all clusters (Fig. 4A, Table S7).
291 Approximately 25% of the edges had TFs and targets assigned to the same WGCNA clade, while
292 the remaining 75% were assigned to different WGCNA clades (Fig. 4B). Given the number of
293 clades identified, the amount of WGCNA same-clade co-assignment is significantly higher than
294 would be expected by chance (z-score ~49). The enrichment for similar expression patterns within
295 TF-target edges suggests we have captured more instances of transcriptional activation than
296 repression, as TF and target expression patterns which would naturally fall into different clades
297 under repressive activity.

298

299 GRN target sets in individual clusters were broadly enriched for photosynthetic and circadian GO
300 terms (Fig. 4C), reflective of the strong regulatory control the clock exerts on the timing of
301 photosynthetic activity and other rhythmic processes (52, 59–61). Comparison of the GRNs
302 between clusters identified generally larger target overlaps between clusters of similar cell types
303 (Fig. 4D), supporting that different cell types within a common tissue maintain some amount of
304 shared network structure. Enrichment was also identified for a number of environmental

305 responsive terms, including temperature and light responses. Given that both light and temperature
306 are key zeitgebers in plant circadian entrainment (62), examining the specific interactions
307 underlying these enrichments could provide new insights into how clock entrainment is maintained
308 in diverse cell types.
309
310 Many TFs had targets identified across multiple clusters, including CCA1, which had predicted
311 targets in 18 of the 19 analyzed clusters. We observed that CCA1-centered networks were also
312 more similar within similar cell types, with Jaccard index based hierarchical clustering
313 highlighting the similarity within mesophyll clusters and vascular clusters (Fig. 4E). This
314 relationship was also seen in other clock components, such as LNK2, PRR7, and TOC1; however,
315 clock components identified as cycling in fewer clusters, such as LNK3 or ELF3, tended to only
316 share overlap in mesophyll associated clusters (Fig. S6).
317
318 To validate our approach for generating TF-resolved scGRNs, we first investigated overlap of
319 CCA1 and PRR7 edges with previously published ChIP-seq datasets, identifying many
320 overlapping targets and highlighting a subset of interactions for evaluation (Fig. 5A). Examination
321 of shared targets of CCA1 between pairs of clusters revealed that the similarity between CCA1-
322 centered networks was largely driven by which and how many photosynthesis-associated targets
323 were identified (Fig. 5B). A suite of 11 light-harvesting chlorophyll a/b-binding proteins (LHCB)
324 with CCA1 edges spanned at least 3 clusters, whereas 7 of the 9 CCA1 edges found in only one or
325 two clusters were associated with Photosystem II repair, with 6 of these 20 CCA1-target pairs (Fig.
326 5B) supported by ChIP-seq binding (63). The combined action of broad light harvesting influence

327 and cell-type-specific PSII repair targets of CCA1 highlight the complex and layered regulation
328 by the clock to fine-tune photosynthetic activity.
329
330 In addition to the similarity of photosynthesis-associated targets across clusters, we also noted that
331 auxin responsive genes in CCA1-centered networks contained a high proportion of edges restricted
332 to a single cluster (Fig. 5C). More than 20% of all genes assigned to auxin-responsive GO
333 categories were identified in CCA1-centered networks in at least one cluster, with edges called
334 between CCA1 and 64 unique targets. A majority of these CCA1-target pairs were identified in
335 Photosynthetic Clusters c0 and c1; however, 13 pairs were unique to clusters other than c0 or c1,
336 and an additional 21 pairs were present in at least one non-Photosynthetic cluster. To further
337 support these TF-target connections, we again leveraged previously published CCA1 ChIP-seq
338 experiments (63), identifying a subset of 18 TF-target edges supported by bulk ChIP-seq binding
339 (Fig. 5C). Given the single cell nature of our dataset, we were curious if we could identify instances
340 of cell-type-specific CCA1 activity. While many of these ChIP-validated edges were only found
341 in Photosynthetic cells, more than half were also present in at least one other cell type. Because
342 our initial scGRN construction was constrained to only cycling genes in each specific cluster, we
343 noted genes which were included in network construction in at least one other cluster (Fig. S7),
344 identifying a total of 10 CCA1 target genes that were included in scGRN construction for more
345 clusters than included an identified CCA1 edge.
346
347 Examination of the PRR7-centered networks identified many edges associated with red light
348 signaling and abscisic acid signaling (Fig. 5D-E). Similar to the CCA1 photosynthesis network,
349 we observed predicted regulation of light harvesting complex (LHC) components by PRR7 across

350 many clusters (Fig. 5D). A majority of these PRR7-*LHC* edges were supported by previously
351 published ChIP-seq binding data (64), again highlighting the strong connection between the
352 circadian clock and the daily timing of photosynthetic capacity. Among edges detected only in one
353 or two clusters, we observed several well-described light signaling components, including targets
354 implicated as PRR7 bound in the referenced ChIP-seq dataset, such as *ELONGATED*
355 *HYPOCOTYL5 (HY5)* and *SUPPRESSOR OF PHYA-105 1 (SPA1)*. Similar to CCA1-centered
356 networks, a majority of the edges identified in more than two clusters were associated with light
357 harvest and capture, again highlighting the fundamental role of the clock in properly timing
358 photosynthetic capacity.
359
360 The ABA-associated *PRR7* network, again similar to the photosynthesis-associated *CCA1*
361 network, contained a large proportion of edges identified in only one cluster. Of note is an edge
362 identified between *PRR7* and *GIBBERELLIC ACID INSENSITIVE (GAI)* in the Epidermal Cluster
363 2, where GA has well defined roles in regulating organ growth and physiology (65, 66). More
364 than half of the multi-cluster edges were also identified as PRR7 bound promoters in the referenced
365 ChIP-seq dataset, including robust, wide-spread regulation of a suite of expected clock
366 components (Fig. 5E). These *PRR7* links to *CCA1, LHY, RVE2, RVE8,* and *ELF3* support that the
367 scGRNs constructed and analyzed in this work have captured biologically relevant interactions
368 between circadian regulated TFs and their varied targets across cell types.
369
370 **Discussion**
371 Unlike animals, plants lack a central nervous system, leading to a long-standing effort to uncover
372 the nature of intercellular communication of circadian clocks in plants. Prior studies have

373 demonstrated that Arabidopsis certain cell types have autonomous clocks that can anticipate
374 environmental inputs and regulate responses (34, 35, 37, 67, 68). To understand the nuances of the
375 cell specific role of the circadian oscillator we conducted a single-nucleus RNA-sequencing
376 (snRNA-seq) time course experiment and constructed cell-type-specific circadian scGRNs. In this
377 study we captured ~30,000 nuclei and were able to identify all major cell types that have been
378 identified in previous single cell/nuclei expression studies of leaf tissue (49, 69, 70). This allowed
379 us to identify cell-type-specific circadian regulated gene expression. As reported in earlier
380 investigations, around 30% of the Arabidopsis transcriptome is circadian regulated with time of
381 day dependent expression patterns (48, 52, 53, 71). Not surprisingly, many of the marker genes
382 commonly used for cell-type-identification during cluster annotation (49, 69, 70) have been shown
383 to be circadian regulated (48). The substantial proportion of marker genes with circadian
384 expression patterns affected our ability to integrate the time course data into cell-type-specific
385 clusters (Fig. 1B). To resolve the cell-type-identities of the clusters, we decided to mask rhythmic
386 genes from integration anchors to identify and annotate clusters in our time series experiment.
387
388 Following cell-type-clustering, we resolved 20 cluster populations, identified by previously
389 reported marker genes and validated by GO analysis (Fig. 1D-F). The clusters were further
390 grouped into five major cell types (Fig. 1D): Mesophyll (M), Epidermis (E), Dividing cells (D),
391 Vasculature (V) and Root Hair (RH). Although in our sampling approach we aimed to enrich the
392 above ground tissue, identification of low numbers of RH cells supports our annotation strategy
393 and its ability to pull out even small populations of cells with distinct identity. Our pseudo-bulk
394 analysis shows cycling of *CCA1*, *LHY*, *PRRs*, *RVEs*, *LNKs* and other clock genes (Fig. 2A) with
395 peak expression at their expected time of the day based on previous bulk RNA-seq studies (72).

396 Our cycling analysis of individual clusters revealed that many of these core clock genes cycle in
397 many clusters (Fig. 2B). For example, *CCA1* cycled in all but one cluster, and *TOC1* and *LHY*
398 cycled in the vast majority of clusters (Fig. 2D). Therefore, our data suggest that a subset of core
399 clock components oscillate robustly in all cell types and support the presence of a functional clock
400 across leaf cell types.
401
402 To be confident in the set of genes defined as rhythmic in our clusters we used WGCNA (56) to
403 group genes with similar temporal expression patterns. We generated 26 network modules which
404 were further grouped into five clades. All five-clades had distinct expression patterns and captured
405 major phases of circadian rhythmic expression pattern throughout the day. Clades 5 and 3 capture
406 the phase of morning expressed genes, clade 2 and 1 consist of genes that have midday expression
407 patterns and clade 4 consists of evening expressed genes. Both *CCA1* and *LHY* were found in
408 clade 3 and 5, consistent with their known dawn/morning phase of expression (18, 73). Similarly,
409 *PRR9* and *PRR7* in clade 2/3, *PRR5* in clade 2/1, *PRR3* in clade 1/2 and *TOC1* in clade 4/1.
410
411 The GO enrichment of our temporal clades further validates previously known circadian regulation
412 of physiological processes. Early morning clades were enriched for auxin response coinciding with
413 previous findings that auxin responses are clock gated and that the amplitude of expression of
414 auxin response genes declines from morning to dusk and then increases from dusk to dawn (74,
415 75). Similarly, the clock plays an important role in regulating ABA and stomatal responses (76).
416 We found enrichment of these responses particularly in the late night clade (Fig. 3A). We also
417 identified enrichment of salicylic acid (SA) mediated signalling pathways in our morning clade in

418 accordance with previous findings that SA peaks in the middle of night and prepares plants for the
419 immune response at dawn when plants are highly vulnerable to pathogen infection (77–79).
420
421 In our analysis, we identified genes cycling across multiple clusters that were segregated into two
422 or more clades, suggesting altered circadian regulation of the same gene across cell types (Fig. 3C-
423 D). Our approach to scGRN construction was to develop individual networks for each cluster using
424 only cycling gene expression (Fig. 4A). This allowed us to temporarily mask the influence of cell-
425 type-specific regulation during network construction, and then regain it through comparison of
426 cluster-resolved networks. We observed that many of the edges for CCA1 and PRR7 overlapped
427 with ChIP-seq predicted targets for each TF, supporting the fact that we have captured biologically
428 relevant interactions in our networks (Fig. 5A). Interestingly, when comparing genes that were
429 regulated across multiple clusters to genes regulated only in a single cluster, we identified broad
430 regulation by CCA1 on light harvesting components, compared to more limited regulation by
431 CCA1 on photosystem II repair components (Fig. 5B). One possible explanation is that the distinct
432 mesophyll clusters we have identified are being clustered at least in part by their photosynthetic
433 status; however, GO enrichment on cluster biomarker sets identified a significant enrichment for
434 PSII repair terms in only one of five mesophyll clusters (Cluster 1, Table S1).
435
436 Direct links tying the circadian clock to steady state PSII repair cycles are largely missing;
437 however, endogenous cycling of phosphorylation status of repair components has been
438 documented, with the key phosphorylation status regulators *STATE TRANSITION8 (STT8), STT8*
439 *HOMOLOG7 (STN7),* and *psbO* all showing circadian expression patterns (71, 80, 81).
440 Additionally, clock gating of PSII repair components has been described in response to stress

441 conditions, including gating of *SIGMA FACTOR5 (SIG5)*, a key regulator of the psbDC operon
442 that is involved in D protein cycling (82–84). The nuclear encoded protease *DEGRADATION OF*
443 *PERIPLASMIC PROTEINS 8 (DEG8)* which is also involved in D protein cycling, was identified
444 as a CCA1 target through scGRN predictions, and is supported by previously published CCA1
445 ChIP-seq binding. Further examination of the relationship between CCA1 and DEG8 could
446 solidify a regulatory link between the clock and steady state PSII repair cycles.
447
448 Alongside a significant role in optimizing the timing of expression of photosynthetic genes, the
449 circadian clock is also intimately linked with auxin (Fig. 5C), having been shown to gate the
450 biosynthesis, transport, and sensitivity to auxin within the plant (75, 85). This relationship between
451 the clock and auxin occurs across many cell types (75, 86), but details of cell-type-specific clock
452 regulation of auxin signalling remains largely unknown. A recent study examined circadian gene
453 expression in Arabidopsis seedlings at the single nucleus resolution, identifying a subset of six
454 *SAUR* genes cycling exclusively in the shoot epidermis (44). Our scGRN-based approach
455 identified 64 auxin-associated CCA1 targets across all clusters, including a subset of 21 genes
456 previously identified as potential CCA1 targets through bulk ChIP-seq. Many of these genes
457 robustly cycle in multiple clusters, yet lack predicted CCA1 regulation outside of a single cluster,
458 suggesting a cell-type-specific regulatory function that has been missed in bulk analyses. One
459 example matching these criteria is *SMALL AUXIN UPREGULATED 15* (*SAUR15*) (63, 87), a
460 ChIP-seq validated CCA1 target that is predicted to be CCA1 regulated in Photosynthetic c1, but
461 not in Vascular c5 or Phloem Companion Cells c6. Similarly, *FLAVODOXIN-LIKE QUINONE*
462 *REDUCTASE 1* (*FQR1*) is a ChIP-seq validated CCA1 target, and edges between the two were
463 predicted in Photosynthetic c0 and Mesophyll c4, but not in Vascular c5 or Guard Cell c14. These

464 interactions capture potential CCA1 regulation of target genes in a cell-type-specific manner, and
465 begin to describe the multifaceted ways in which the clock coordinates auxin signaling across the
466 mature Arabidopsis leaf.
467
468 We closely examined a handful of PRR7-centered networks due to the promising overlap between
469 *PRR7* scGRN targets and previously published target promoters of PRR7 identified through ChIP
470 (Fig. 5A). *PRR7* serves as a crucial link between the circadian clock and light signaling pathways.
471 Along with *PRR9*, *PRR7* participates in clock entrainment by red light, where *PHYTOCHROME*
472 *B (PHYB)* provides input into the clock partially through the PRRs (64, 88, 89). Consistent with
473 this, our snGRN analysis revealed that PRR7 regulatory targets contain many red light response
474 components (Fig. 5D). *PRR7* was predicted to regulate numerous light-responsive genes across
475 cell types, including key photomorphogenic regulators such as *HY5* and *SPA1*, which are central
476 to red/far-red light signaling and cell elongation in the hypocotyl (90, 91). *PRR7* connections to
477 *HY5* were identified in both mesophyll and epidermal clusters, while *SPA1* connections were
478 exclusively found in mesophyll clusters, suggesting additional regulators might contribute to
479 circadian control of *SPA1* transcription. Many of the *PRR7* target interactions were supported by
480 prior *PRR7* ChIP-seq binding data (Fig. 5A), indicating that PRR7 directly links the clock to genes
481 governing light perception and response. The presence of PRR7–*LHC* (light-harvesting
482 chlorophyll complex) edges in multiple clusters further highlights a role for *PRR7* in gating
483 photosynthetic light capture to specific times of day. Together, these findings suggest *PRR7*
484 enhances environmental responsiveness by synchronizing red light signal transduction with the
485 circadian schedule, thereby optimizing light-dependent processes in a time-of-day specific
486 manner.

487

488 Circadian regulation of hormone signaling pathways, including abscisic acid (ABA) responses, is
489 essential for plant stress adaptation, and PRR7 has emerged as a key clock TF involved in ABA
490 and stress responses (92–94). In our scGRNs, *PRR7*-centered interactions were significantly
491 associated with "response to abscisic acid" gene sets, and these interactions were often highly
492 tissue-specific. For instance, *PRR7* was linked to the DELLA protein gene *GAI* in an epidermis-
493 specific network. *GAI* modulates growth and intersects with ABA in controlling stomatal aperture
494 (95), and an epidermis-only PRR7-*GAI* edge suggests that *PRR7* may gate ABA/GA-dependent
495 stress responses (such as transpiration or growth) in a cell-type-specific manner. These insights
496 align with functional studies showing circadian clock components influence the ABA pathway
497 where the PRR5/7/9 trio negatively regulates ABA biosynthesis and signaling, as a *prr5prr7prr9*
498 triple mutant accumulates more ABA and alters drought responses (96). Indeed, loss of *PRR7*
499 (alone or with other PRRs) affects stress tolerance – for example, *prr5prr7prr9* mutants show
500 enhanced drought and salinity tolerance, reflecting a clock loosened from its usual restraint on
501 stress pathways (97). Thus, PRR7 is a likely candidate to integrate circadian timing with ABA
502 signaling to modulate stress-response genes at the right time and place, optimizing stress resilience
503 without compromising daily growth rhythms.

504

505 This study provides a comprehensive cell-type-resolved view of circadian gene regulation in
506 mature Arabidopsis leaves. Through snRNA-seq profiling across a full 24-hour time course, we
507 reveal widespread circadian regulation across all major tissue types, uncovering over 7,000 genes
508 with rhythmic expression and demonstrating that core oscillator components are active and cycling
509 in nearly all clusters. By integrating coexpression-based phase assignment and constructing

510 cluster-specific gene regulatory networks, we identified both broadly shared and cell-type–
511 restricted transcriptional programs. In particular, we show that key clock regulators such as CCA1
512 exhibit distinct regulatory wiring across tissues, targeting photosynthesis- and auxin-associated
513 genes in a cell-type-specific manner. Ultimately, our work highlights the importance of cell-type-
514 context in shaping circadian outputs and lays a foundation for future efforts to manipulate temporal
515 regulation in a tissue-targeted manner.
516

517 **Material and Methods**

518 **Plant Growth and Sampling**

519 Arabidopsis Col seeds were surface sterilized for four hours by vapor phase sterilization (98).
520 Sterilized seeds were imbibed with water. Seeds were plated on half strength Murashige Skoog
521 (MS) agar with 1% sucrose and a pH of 5.7 buffered with Potassium Hydroxide (KOH). Seeds
522 were then stratified at 4°C for two days in complete darkness. Following stratification plates were
523 placed in a chamber with 12L/12D photoperiod (light intensity 130 μmol s^{-1}) at 22°C. Seedlings
524 were entrained to 12L/12D conditions for 11 days. On the 11th day, starting at subjective dawn,
525 seedlings were grown in constant light for 48 hours before the start of the time course. Leaf samples
526 of 180-250 seedlings were harvested by cutting across the root-shoot junction in 2 replicates for
527 single-nuclei RNA-seq every 4 hours over a 24-hour period starting at the subjective dawn of the
528 13th day.
529

530 **Nuclei Isolation**

531 Leaf tissue was collected in a petri plate containing 5 ml of pre chilled NIB (10mM Tris-HCL-pH
532 7.4, 10 mM NaCl, 3 mM MgCl, 0.5mM Spermidine, 0.2 mM Spermine, 0.5% Bovine Serum

533 Albumin with 1:1000 Roche Complete Protease Inhibitor and 0.03 U/µl of RNase inhibitor but
534 without detergents). Leaf samples were chopped at 4°C for 3 min on a petri plate containing 5 ml
535 of NIB, with a razor blade. Finely chopped leaf samples were then shifted to 50 ml falcon tubes,
536 ~ 15 ml of NIB was added to make the final volume of sample 20 ml. Samples were incubated on
537 a rotating platform for 5 min to facilitate cell release. After the first incubation, samples were
538 filtered via 70 µm and 40 µm cell strainers to remove leaf debris. Triton X-100 and NP-40 were
539 added to final concentration of 0.05% and extracts were incubated on a rotating platform at 4°C
540 for 10 min. The nuclei suspension was then centrifuged at 500 x g for 5 min at 4°C. The nuclei
541 pellet was then resuspended in 5 ml of NIB without detergents and was again pelleted at 500 x g
542 for 5 min at 4°C. The pellet was resuspended in 750 µl of resuspension buffer (1X PBS + 1% BSA
543 + 0.03 U/ul RNaseI). Nuclei suspension was then shifted to the Nuclei Isolation column and
544 collection tube of the Chromium nuclei isolation kit (PN-10000494, 10X Genomics, Pleasanton
545 CA). Samples were then centrifuged at 16000 x g for 40 seconds. Pelleted nuclei were finally
546 resuspended in 500 µl of resuspension buffer. Nuclei were counted manually with a
547 hemocytometer. The 32k nuclei were loaded onto the 10x Genomics Chip M, which was then
548 processed with 10x Genomics Chromium X controller, and sequencing libraries were constructed
549 following manufacturer's instructions except for cDNA amplification step where 13 cycles were
550 used i.e. 2 additional cycles to prepare cDNA from nuclei (PN-1000268 number for the kit, 10X
551 Genomics, Pleasanton CA). Total time from leaf harvest to loading was 30-40 min.
552

553 **Data Analysis**

554 Cell Ranger (v7.0.1) was used to generate gene by cell matrices from Demultiplexed FASTQ files
555 by aligning with Arabidopsis TAIR10 genome. Downstream analyses were performed with Seurat

556 (v5.1.0). Cells with low numbers of UMIs or plastid contamination were removed using Median
557 Absolute Deviation filtering (filterbyMAD.R), and potential doublets were identified and removed
558 through scDblFinder version 1.2 (99).
559
560 After initial filtering and discarding low quality cells, the data were normalized by using the
561 "LogNormalize" global scaling method. Following normalization, highly variable features were
562 computed for cells of the dataset. We then used Principal Component Analysis for linear
563 transformation and linear dimensionality reduction. After identifying the significant PCs, we
564 implemented a graph-based clustering algorithm. Cells were embedded in a K-nearest neighbor
565 graph structure, with cells of similar expression patterns having edges drawn to connect them
566 followed by partitioning into communities. For clustering the cells, the Louvain algorithm was
567 applied based on 30 top PCs.
568
569 Pseudo bulk samples were generated by aggregating the raw counts at sample and cluster level to
570 identify oscillating gene expression. We used DeSeq2 to generate the normalized count matrix.
571 For detecting expression of genes that oscillate throughout the time course we used METACYCLE
572 (100). METACYCLE uses three different cycling detection algorithms i.e. meta2d: integrated
573 ARSE, JTK-CYCLE and LS. We utilized JTK-CYCLE output to identify genes whose expression
574 oscillates by setting cut-off Adj p-value < 0.05. The number of oscillating genes that were either
575 specific to a cluster or shared between different clusters were illustrated by UpSet plots using the
576 package UpSetR implemented under the *R* environment (101). JTK-CYCLE accurately measures
577 the phase, period, and amplitude. We used phase information for each gene and calculated phase

578 difference of genes that were shared between different clusters to identify genes that were
579 oscillating with different phases in between different clusters.
580
581 **WGCNA analysis**
582 To validate the phase difference observed, we used the WGCNA package (56) to analyze genes
583 for all clusters together by including a cluster identifier appended to the gene name. A total of
584 13,552 genes were fed into WGCNA. To identify module based correlation, a soft threshold of 30
585 was used. WGCNA identified 26 modules, genes with similar expression patterns were clustered
586 together in the same module, whereas those with different phases segregated out into different
587 modules. We further filtered the modules based on Module Eigengene connectivity (kME),
588 removing any gene with a kME $\geq$ 0.6. Additionally, to group similar modules together, we
589 calculated the correlation matrix of the average zScores of all the modules and performed
590 hierarchical clustering to identify major clades or expression patterns. This resulted in five
591 modules with distinct temporal expression patterns. All code used for this analysis can be found
592 on github (https://github.com/GreenhamLab/Arabidopsis_snRNAseq_Circadian_Transcriptome).
593
594 **scGRN Construction**
595 Single cell GRNs were built with SCENIC implementation of GENIE3 (102, 103) by subsetting
596 the single nucleus dataset into individual clusters and proceeding only with data from cycling
597 genes. Several steps of the scGRN construction were adapted from the scPlant R package (104).
598 To identify an appropriate weight threshold for each network, we shuffled and permuted our gene
599 expression matrix into ten iterations, and identified the weight value corresponding to the 95th

percentile for each cluster's aggregated network. This weight was used as a cutoff for our unshuffled networks. Networks were visualized and annotated in Cytoscape (105).

Declarations

Availability of data and materials

All code used to process and analyze the reported data is available at https://github.com/GreenhamLab/Arabidopsis_snRNAseq_Circadian_Transcriptome. Raw sequencing data is available upon publication through SRA through BioProject accession #PRJNA1277851.

Competing interests

The authors declare that they have no competing interests.

Funding

This project was supported by funding from NSF DBI 2042159 to KG and NIH NIGMS 5R35GM14837-03 to AZ, ZAM, AM, and KG. This article was submitted to the bioRxiv preprint server and is hosted under a CC-NY-BC 4.0 International License.

Authors' contributions

AZ, ZAM, and KG designed the experiments. AZ, ZAM, AM, and KG performed the experiments. AZ and ZAM analyzed the data. AZ, ZAM, and KG interpreted the results and wrote the manuscript. All authors read, provided feedback, and approved the final manuscript.

Acknowledgements

This work was supported by the resources and staff at the University of Minnesota Genomics Center who performed all sequencing on this project, and by the resources and staff at the University of Minnesota University Imaging Centers (UIC, SCR_020997) who assisted with sample preparation assessment. We wish to thank Danielle Schoenecker for assistance with plant growth and care, and Rui Kuang and Tianci Song for feedback on data processing approaches.

Figures

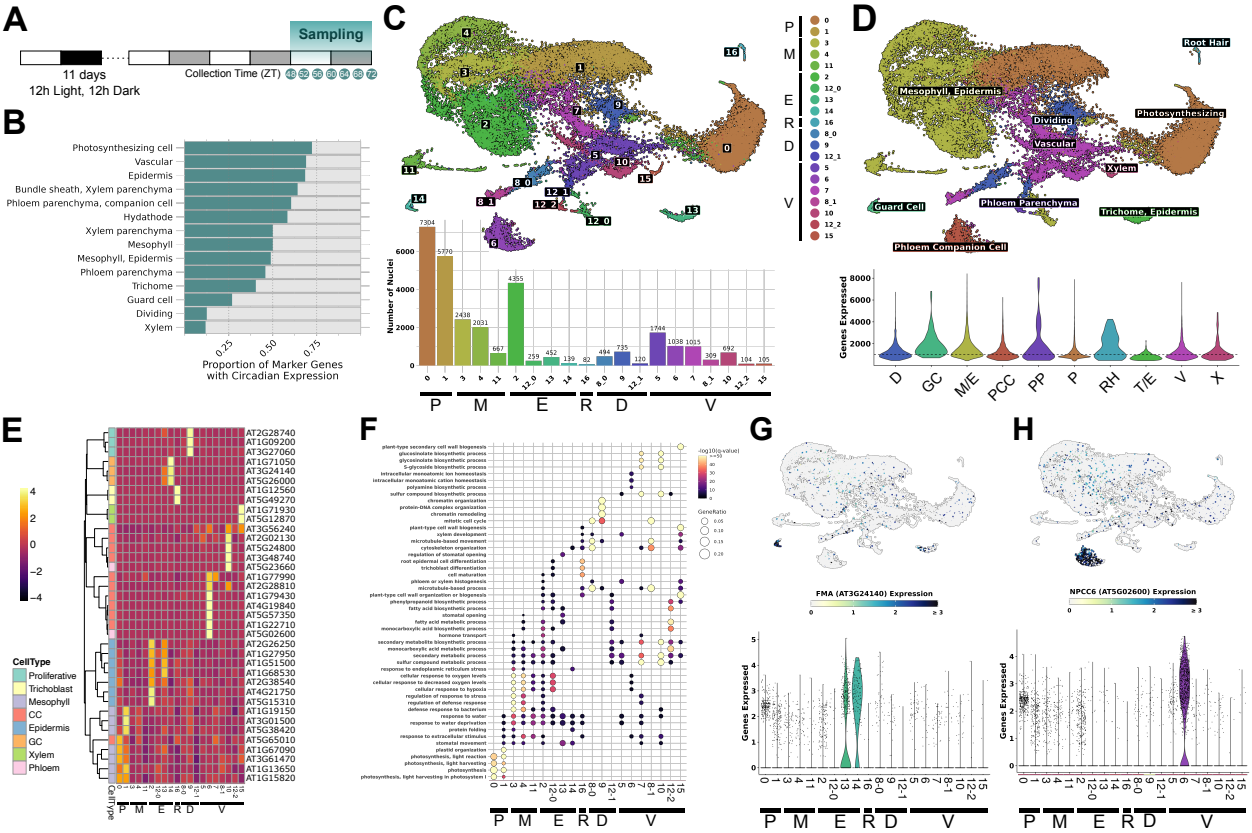

Figure 1. Major cell and tissue types can be resolved in the mature Arabidopsis leaf over a circadian time course. (**A**) Growth and sampling schematic used to generate the snRNA-seq dataset. (**B**) The proportion of cell type marker genes identified that are under circadian regulation. (**C**) UMAP projection of the fully integrated, cycling-masked snRNA-seq dataset (top), and the number of nuclei identified in each cluster (bottom). (**D**) UMAP projection, highlighting broader tissue types alongside more specialized cell types (top), and the violin plots describing the distribution of genes expressed in each group (bottom). (**E**) Scaled expression heatmap of a suite of previously identified cell-type-specific genes across the snRNA-seq time course. (**F**) Gene Ontology biological process enrichments of cluster biomarkers support expected cell-type-specific activities. (**G-H**) Expression feature plots for *FAMA* (FMA, AT3G24140) and *NUCLEAR-*

659 *ENRICHED PHLOEM COMPANION CELL GENE 6* (NPCC6, AT5G02600), significant cluster
660 biomarkers for guard cells (Cluster 14) and phloem companion cells (Cluster 6) respectively. D,
661 Dividing; E, Epidermis; GC, Guard Cell; M, Mesophyll; M/E, Mesophyll/Epidermis; P,
662 Photosynthesizing; PCC, Phloem Companion Cell; PP, Phloem Parenchyma; R, Root; RH, Root
663 Hair; T/E, Trichome/Epidermis; V, Vascular; X, Xylem.
664
665
666
667
668
669
670
671
672
673
674
675
676
677
678
679
680

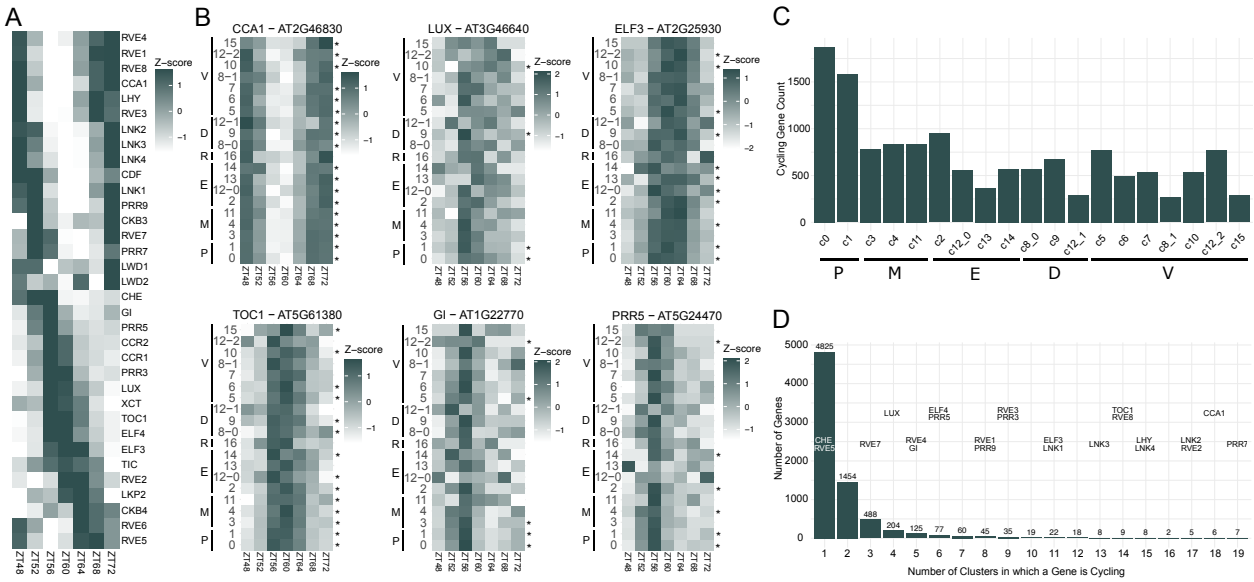

Figure 2. Single nucleus RNA-sequencing captures circadian gene expression across diverse cell types of the mature Arabidopsis leaf. (**A**) Pseudo-bulk expression levels of key clock components and outputs over a circadian day. (**B**) Cluster-resolved expression of *CCA1* (top left), *TOC1* (bottom left), and *LUX* (top center), *GI* (bottom center), *ELF3* (top right), and *PRR5* (bottom right) over a circadian day. Asterisks indicate a significant cycling call in the associated cluster. (**C**) Number of cycling genes identified through CycleJTK in each cluster. (**D**) Distribution of genes based on how many clusters in which they were called cycling. The presence of key clock TFs are indicated above the relevant groups.

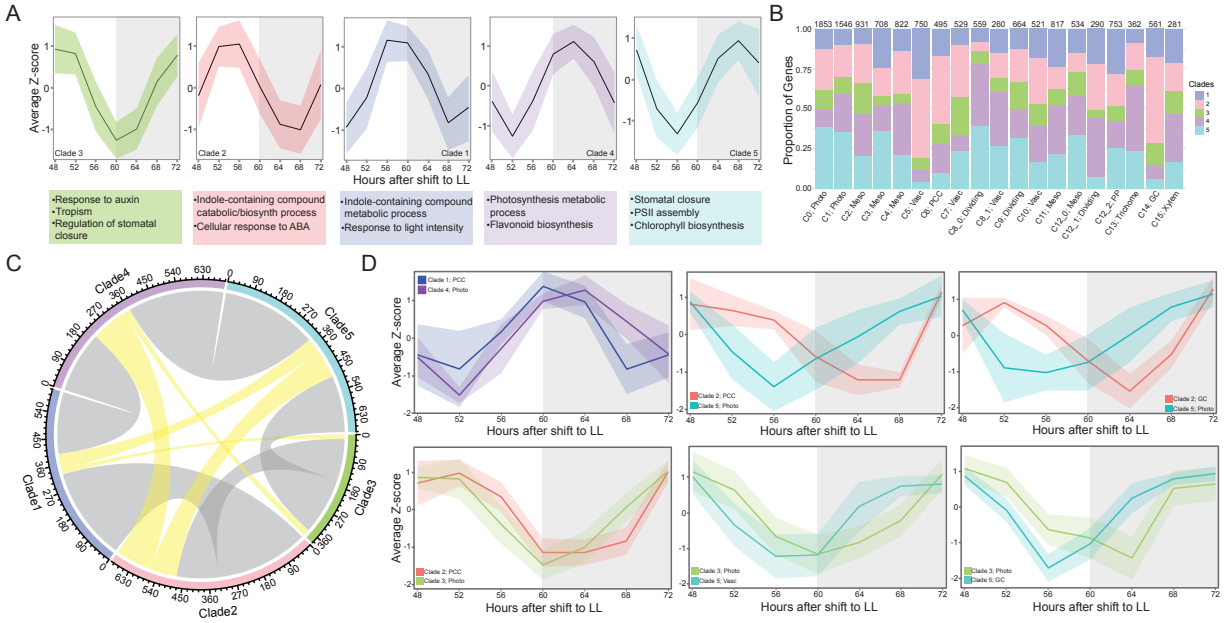

Figure 3. Identification of temporal expression patterns across cell types through WGCNA and characterization of cell-type-specific phase changes in circadian expression. (A) Hierarchical clustering of WGCNA modules identified five major temporal clades. The average zScore for genes in each clade was plotted to get the representative expression pattern across clades. The ribbon represents the standard deviation. A selection of significantly GO enriched terms is included below each clade. (**B**) Proportional distribution of clades across clusters. **(C)** The circos plot shows the genes with a change in phase across two clusters resulting in placement in two different clades. The width of the ribbon signifies the number of genes with a phase change. The grey ribbon shows shifts to the adjacent clades, while the yellow ribbon represents shifts across clades (**D**) Expression pattern differences of sets of genes found cycling across different tissue types. The average zScore of the genes within each cluster is shown to highlight the phase difference. Ribbons represent standard deviation.

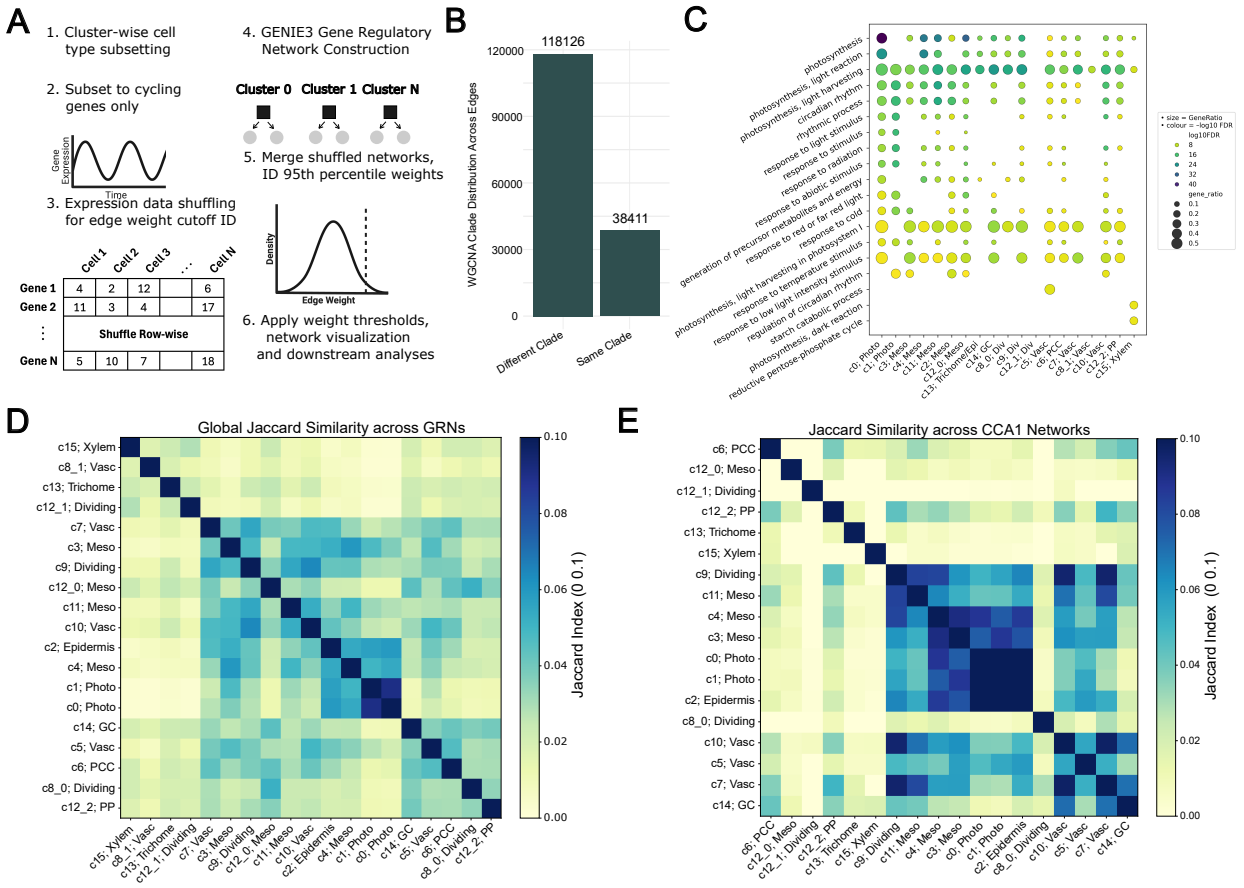

Figure 4. Construction and evaluation of circadian, cluster-resolved single cell gene regulatory networks (scGRNs). (**A**) Schematic detailing the steps used to generate and filter scGRNs. (**B**) Number of scGRN edges where the TF and target are assigned to the same or different WGCNA clades. (**C**) Gene ontology biological process enrichment, showing the top 5 most enriched categories for each cluster. Photo, Photosynthetic; Meso, Mesophyll; Epi, Epidermis; GC, Guard Cell; Div, Dividing; Vasc, Vascular; PCC, Phloem Companion Cell; PP, Phloem Parenchyma. (**D**) Jaccard Index similarity matrix between pairs of clusters, using all significant edges identified. (**E**) Jaccard Index similarity matrix between pairs of clusters, restricted to significant CCA1-centered networks.

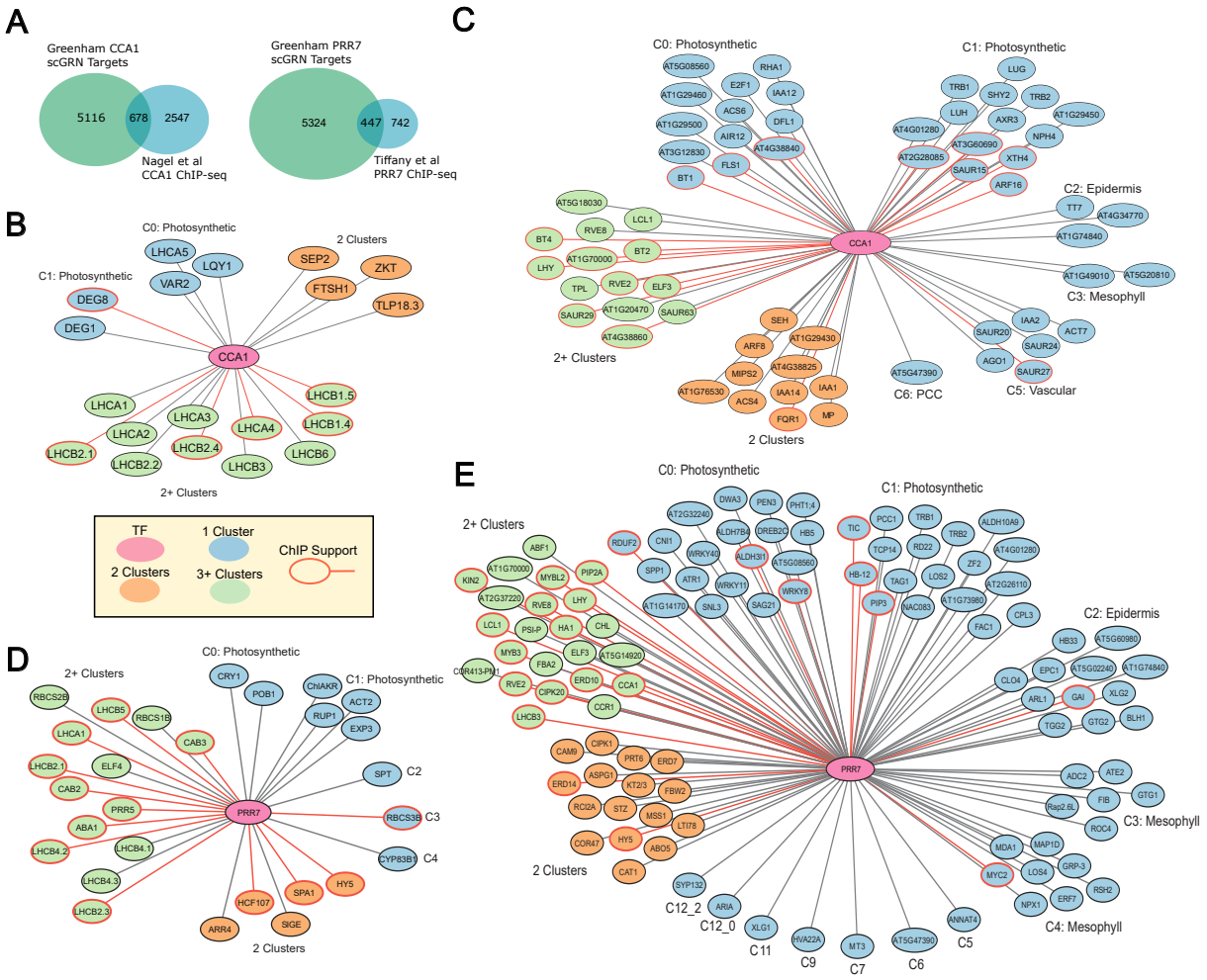

723

724 **Figure 5. Examination of TF-resolved scGRNs for CCA1 and PRR7.** (**A**) Overlap between
725 scGRN edges identified in this study, and targets of CCA1 (left) or PRR7 (right) in previously
726 published ChIP-seq experiments. (**B-E**) Node color indicates how many clusters an edge was
727 identified in. Red edges and borders indicate support for an interaction through previously
728 published ChIP-seq data. (**B**) CCA1-centered network built from all significant edges associated
729 with the Photosynthesis GO:0015979 category. (**C**) CCA1-centered network built from all
730 significant edges associated with the Response to Auxin GO:0009733 category. (**D**) PRR7-
731 centered network built from all significant edges associated with the Response to Red Light

732 GO:0010114 category. (**E**) PRR7-centered network built from all significant edges associated with

733 the Response to Abscisic Acid GO:0009737 category.

734

735

736

737

738

739

740

741

742

743

744

745

746

747

748

749

750

751

752

753

754 **References**

755 1. R. Saini, M. Jaskolski, S. J. Davis, Circadian oscillator proteins across the kingdoms of life:
756 structural aspects. *BMC Biol.* **17**, 13 (2019).

757 2. C. N. Micklem, J. C. W. Locke, Cut the noise or couple up: Coordinating circadian and synthetic
758 clocks. *iScience* **24**, 103051 (2021).

759 3. Y. Ouyang, C. R. Andersson, T. Kondo, S. S. Golden, C. H. Johnson, Resonating circadian clocks
760 enhance fitness in cyanobacteria. *Proc. Natl. Acad. Sci. U. S. A.* **95**, 8660–8664 (1998).

761 4. P. Achermann, H. Kunz, Modeling circadian rhythm generation in the suprachiasmatic nucleus with
762 locally coupled self-sustained oscillators: phase shifts and phase response curves. *J. Biol. Rhythms*
763 **14**, 460–468 (1999).

764 5. S. Adams, I. Manfield, P. Stockley, I. A. Carré, Revised morning loops of the Arabidopsis circadian
765 clock based on analyses of direct regulatory interactions. *PLoS One* **10**, e0143943 (2015).

766 6. M. Akashi, T. Takumi, The orphan nuclear receptor RORα regulates circadian transcription
767 mammalian core-clock Bmal1. *Nature structural & molecular biology* **12**, 441–448 (2005).

768 7. N. R. J. Glossop, P. E. Hardin, Central and peripheral circadian oscillator mechanisms in flies and
769 mammals. *J. Cell Sci.* **115**, 3369–3377 (2002).

770 8. M. H. Hastings, A. B. Reddy, E. S. Maywood, A clockwork web: circadian timing in brain and
771 periphery, in health and disease. *Nat. Rev. Neurosci.* **4**, 649–661 (2003).

772 9. K. Greenham, C. R. McClung, Integrating circadian dynamics with physiological processes in
773 plants. *Nat. Rev. Genet.* **16**, 598–610 (2015).

774 10. A. N. Dodd, *et al.*, Plant circadian clocks increase photosynthesis, growth, survival, and competitive
775 advantage. *Science* **309**, 630–633 (2005).

776 11. A. Graf, A. Schlereth, M. Stitt, A. M. Smith, Circadian control of carbohydrate availability for
777 growth in Arabidopsis plants at night. *Proc. Natl. Acad. Sci. U. S. A.* **107**, 9458–9463 (2010).

778 12. A. Pokhilko, *et al.*, The clock gene circuit in Arabidopsis includes a repressilator with additional
779 feedback loops. *Mol. Syst. Biol.* **8**, 574 (2012).

780 13. M. A. Nohales, S. A. Kay, Molecular mechanisms at the core of the plant circadian oscillator. *Nat.*
781 *Struct. Mol. Biol.* **23**, 1061–1069 (2016).

782 14. C. Strayer, *et al.*, Cloning of the Arabidopsis clock gene TOC1, an autoregulatory response regulator
783 homolog. *Science* **289**, 768–771 (2000).

784 15. N. Nakamichi, *et al.*, PSEUDO-RESPONSE REGULATORS 9, 7, and 5 are transcriptional
785 repressors in the Arabidopsis circadian clock. *Plant Cell* **22**, 594–605 (2010).

786 16. D. Alabadí, *et al.*, Reciprocal regulation between TOC1 and LHY/CCA1 within the Arabidopsis
787 circadian clock. *Science* **293**, 880–883 (2001).

788 17. R. Schaffer, *et al.*, The late elongated hypocotyl mutation of Arabidopsis disrupts circadian rhythms

789 and the photoperiodic control of flowering. *Cell* **93**, 1219–1229 (1998).

790 18. Z. Y. Wang, E. M. Tobin, Constitutive expression of the *CIRCADIAN CLOCK ASSOCIATED 1*
791 (*CCA1*) gene disrupts circadian rhythms and suppresses its own expression. *Cell* **93**, 1207–1217
792 (1998).

793 19. Q. Xie, *et al.*, LNK1 and LNK2 are transcriptional coactivators in the Arabidopsis circadian
794 oscillator. *Plant Cell* **26**, 2843–2857 (2014).

795 20. D. A. Nusinow, *et al.*, The ELF4-ELF3-LUX complex links the circadian clock to diurnal control of
796 hypocotyl growth. *Nature* **475**, 398–402 (2011).

797 21. M. L. Rugnone, *et al.*, LNK genes integrate light and clock signaling networks at the core of the
798 Arabidopsis oscillator. *Proc. Natl. Acad. Sci. U. S. A.* **110**, 12120–12125 (2013).

799 22. R. Rawat, *et al.*, REVEILLE8 and PSEUDO-REPONSE REGULATOR5 form a negative feedback
800 loop within the Arabidopsis circadian clock. *PLoS Genet.* **7**, e1001350 (2011).

801 23. B. Farinas, P. Mas, Functional implication of the MYB transcription factor RVE8/LCL5 in the
802 circadian control of histone acetylation: Role of RVE8/LCL5 in the circadian clock. *Plant J.* **66**,
803 318–329 (2011).

804 24. Y. Wang, *et al.*, LIGHT-REGULATED WD1 and PSEUDO-RESPONSE REGULATOR9 form a
805 positive feedback regulatory loop in the Arabidopsis circadian clock. *Plant Cell* **23**, 486–498 (2011).

806 25. J.-F. Wu, *et al.*, LWD-TCP complex activates the morning gene CCA1 in Arabidopsis. *Nat.*
807 *Commun.* **7**, 13181 (2016).

808 26. M. Ma, H. Elizabeth, *Neuroanatomy, nucleus suprachiasmatic* (2019).

809 27. P. D. Gould, *et al.*, Coordination of robust single cell rhythms in the Arabidopsis circadian clock via
810 spatial waves of gene expression. *Elife* **7** (2018).

811 28. N. Takahashi, Y. Hirata, K. Aihara, P. Mas, A hierarchical multi-oscillator network orchestrates the
812 Arabidopsis circadian system. *Cell* **163**, 148–159 (2015).

813 29. H. Ikeda, *et al.*, Circadian clock controls root hair elongation through long-distance communication.
814 *Plant Cell Physiol.* **64**, 1289–1300 (2023).

815 30. Y. Li, *et al.*, Molecular investigation of organ-autonomous expression of Arabidopsis circadian
816 oscillators: Organ-autonomous expression of clock oscillators. *Plant Cell Environ.* **43**, 1501–1512
817 (2020).

818 31. M. Endo, H. Shimizu, M. A. Nohales, T. Araki, S. A. Kay, Tissue-specific clocks in Arabidopsis
819 show asymmetric coupling. *Nature* **515**, 419–422 (2014).

820 32. H. Shimizu, *et al.*, Decentralized circadian clocks process thermal and photoperiodic cues in specific
821 tissues. *Nat. Plants* **1**, 15163 (2015).

822 33. U. Voß, *et al.*, The circadian clock rephases during lateral root organ initiation in *Arabidopsis*
823 *thaliana*. *Nat. Commun.* **6**, 7641 (2015).

824 34. S. C. Thain, A. Hall, A. J. Millar, Functional independence of circadian clocks that regulate plant

825 gene expression. *Curr. Biol.* **10**, 951–956 (2000).

826 35. A. B. James, *et al.*, The circadian clock in Arabidopsis roots is a simplified slave version of the clock
827 in shoots. *Science* **322**, 1832–1835 (2008).

828 36. B. Wenden, D. L. K. Toner, S. K. Hodge, R. Grima, A. J. Millar, Spontaneous spatiotemporal waves
829 of gene expression from biological clocks in the leaf. *Proc. Natl. Acad. Sci. U. S. A.* **109**, 6757–6762
830 (2012).

831 37. M. Greenwood, M. Domijan, P. D. Gould, A. J. W. Hall, J. C. W. Locke, Coordinated circadian
832 timing through the integration of local inputs in Arabidopsis thaliana. *PLoS Biol.* **17**, e3000407
833 (2019).

834 38. H. Fukuda, N. Nakamichi, M. Hisatsune, H. Murase, T. Mizuno, Synchronization of plant circadian
835 oscillators with a phase delay effect of the vein network. *Phys. Rev. Lett.* **99**, 098102 (2007).

836 39. E. Yakir, *et al.*, Cell autonomous and cell-type specific circadian rhythms in Arabidopsis. *Plant J.*
837 **68**, 520–531 (2011).

838 40. R. Shahan, *et al.*, A single-cell Arabidopsis root atlas reveals developmental trajectories in wild-type
839 and cell identity mutants. *Dev. Cell* **57**, 543–560.e9 (2022).

840 41. X. Guo, *et al.*, An Arabidopsis single-nucleus atlas decodes leaf senescence and nutrient allocation.
841 *Cell* **188**, 2856–2871.e16 (2025).

842 42. C. B. Lopez-Anido, *et al.*, Single-cell resolution of lineage trajectories in the Arabidopsis stomatal
843 lineage and developing leaf. *Dev. Cell* **56**, 1043–1055.e4 (2021).

844 43. F. Apelt, *et al.*, Shoot and root single cell sequencing reveals tissue- and daytime-specific
845 transcriptome profiles. *Plant Physiol.* **188**, 861–878 (2022).

846 44. Y. Qin, *et al.*, 48-hour and 24-hour time-lapse single-nucleus transcriptomics reveal cell-type
847 specific circadian rhythms in Arabidopsis. *Nat. Commun.* **16**, 4171 (2025).

848 45. G. X. Y. Zheng, *et al.*, Massively parallel digital transcriptional profiling of single cells. *Nat.*
849 *Commun.* **8**, 14049 (2017).

850 46. K. Wang, *et al.*, An optimized FACS-free single-nucleus RNA sequencing (snRNA-seq) method for
851 plant science research. *Plant Sci.* **326**, 111535 (2023).

852 47. S. ’ang Wen, *et al.*, Spatiotemporal single-cell analysis of gene expression in the mouse
853 suprachiasmatic nucleus. *Nat. Neurosci.* **23**, 456–467 (2020).

854 48. A. Romanowski, R. G. Schlaen, S. Perez-Santangelo, E. Mancini, M. J. Yanovsky, Global
855 transcriptome analysis reveals circadian control of splicing events in Arabidopsis thaliana. *Plant J.*
856 **103**, 889–902 (2020).

857 49. T. A. Lee, *et al.*, A single-nucleus atlas of seed-to-seed development in Arabidopsis. *bioRxiv*
858 2023.03.23.533992 (2023).

859 50. D. C. Bergmann, W. Lukowitz, C. R. Somerville, Stomatal development and pattern controlled by a
860 MAPKK kinase. *Science* **304**, 1494–1497 (2004).

861 51. C. Zhang, R. A. Barthelson, G. M. Lambert, D. W. Galbraith, Global characterization of cell-specific
862 gene expression through fluorescence-activated sorting of nuclei. *Plant Physiol.* **147**, 30–40 (2008).

863 52. S. L. Harmer, *et al.*, Orchestrated transcription of key pathways in Arabidopsis by the circadian
864 clock. *Science* **290**, 2110–2113 (2000).

865 53. M. F. Covington, J. N. Maloof, M. Straume, S. A. Kay, S. L. Harmer, Global transcriptome analysis
866 reveals circadian regulation of key pathways in plant growth and development. *Genome Biol.* **9**,
867 R130 (2008).

868 54. M. E. Hughes, J. B. Hogenesch, K. Kornacker, JTK_CYCLE: an efficient nonparametric algorithm
869 for detecting rhythmic components in genome-scale data sets. *J. Biol. Rhythms* **25**, 372–380 (2010).

870 55. M. E. Hughes, *et al.*, Guidelines for genome-scale analysis of biological rhythms. *J. Biol. Rhythms*
871 **32**, 380–393 (2017).

872 56. P. Langfelder, S. Horvath, WGCNA: an R package for weighted correlation network analysis. *BMC*
873 *Bioinformatics* **9**, 559 (2008).

874 57. K. Greenham, *et al.*, Temporal network analysis identifies early physiological and transcriptomic
875 indicators of mild drought in Brassica rapa. *Elife* **6**, e29655 (2017).

876 58. K. Greenham, *et al.*, Expansion of the circadian transcriptome in *Brassica rapa* and genome-wide
877 diversification of paralog expression patterns. *Elife* **9**, e58993 (2020).

878 59. A. N. Dodd, N. Dalchau, M. J. Gardner, S.-J. Baek, A. A. R. Webb, The circadian clock has transient
879 plasticity of period and is required for timing of nocturnal processes in Arabidopsis. *New Phytol.*
880 **201**, 168–179 (2014).

881 60. M. J. Haydon, O. Mielczarek, F. C. Robertson, K. E. Hubbard, A. A. R. Webb, Photosynthetic
882 entrainment of the *Arabidopsis thaliana* circadian clock. *Nature* **502**, 689–692 (2013).

883 61. T. L. Hennessey, C. B. Field, Circadian rhythms in photosynthesis : Oscillations in carbon
884 assimilation and stomatal conductance under constant conditions: Oscillations in carbon assimilation
885 and stomatal conductance under constant conditions. *Plant Physiol.* **96**, 831–836 (1991).

886 62. S. Wang, G. Steed, A. A. R. Webb, Circadian entrainment in Arabidopsis. *Plant Physiol.* **190**, 981–
887 993 (2022).

888 63. D. H. Nagel, *et al.*, Genome-wide identification of CCA1 targets uncovers an expanded clock
889 network in Arabidopsis. *Proc. Natl. Acad. Sci. U. S. A.* **112**, E4802–10 (2015).

890 64. T. L. Liu, L. Newton, M.-J. Liu, S.-H. Shiu, E. M. Farré, A G-box-like motif is necessary for
891 transcriptional regulation by circadian pseudo-response REGULATORs in Arabidopsis. *Plant*
892 *Physiol.* **170**, 528–539 (2016).

893 65. S. Sauret-Güeto, G. Calder, N. P. Harberd, Transient gibberellin application promotes *Arabidopsis*
894 *thaliana* hypocotyl cell elongation without maintaining transverse orientation of microtubules on the
895 outer tangential wall of epidermal cells: Gibberellins and microtubule orientation. *Plant J.* **69**, 628–
896 639 (2012).

897 66. C.-H. Goh, D. J. Lee, H.-J. Bae, Gibberellic acid of Arabidopsis regulates the abscisic acid-induced
898 inhibition of stomatal opening in response to light. *Plant Sci.* **176**, 136–142 (2009).

899 67. S. Bordage, S. Sullivan, J. Laird, A. J. Millar, H. G. Nimmo, Organ specificity in the plant circadian
900 system is explained by different light inputs to the shoot and root clocks. *New Phytol.* **212**, 136–149
901 (2016).

902 68. H. G. Nimmo, Entrainment of Arabidopsis roots to the light:dark cycle by light piping. *Plant Cell*
903 *Environ.* **41**, 1742–1748 (2018).

904 69. Y. Wang, Q. Huan, K. Li, W. Qian, Single-cell transcriptome atlas of the leaf and root of rice
905 seedlings. *J. Genet. Genomics* **48**, 881–898 (2021).

906 70. K. Xia, *et al.*, The single-cell stereo-seq reveals region-specific cell subtypes and transcriptome
907 profiling in Arabidopsis leaves. *Dev. Cell* **57**, 1299–1310.e4 (2022).

908 71. K. D. Edwards, *et al.*, FLOWERING LOCUS C mediates natural variation in the high-temperature
909 response of the Arabidopsis circadian clock. *Plant Cell* **18**, 639–650 (2006).

910 72. P. Y. Hsu, S. L. Harmer, Wheels within wheels: the plant circadian system. *Trends Plant Sci.* **19**,
911 240–249 (2014).

912 73. R. Schaffer, *et al.*, Microarray analysis of diurnal and circadian-regulated genes in Arabidopsis.
913 *Plant Cell* **13**, 113 (2001).

914 74. X. Xue, K. Sun, Z. Zhu, CIRCADIAN CLOCK ASSOCIATED 1 gates morning phased auxin
915 response in *Arabidopsis thaliana*. *Biochem. Biophys. Res. Commun.* **527**, 935–940 (2020).

916 75. M. F. Covington, S. L. Harmer, The circadian clock regulates auxin signaling and responses in
917 Arabidopsis. *PLoS Biol.* **5**, e222 (2007).

918 76. K. E. Hubbard, A. A. R. Webb, "Circadian rhythms in stomata: Physiological and molecular
919 aspects" in *Rhythms in Plants*, (Springer International Publishing, 2015), pp. 231–255.

920 77. M. Melotto, W. Underwood, J. Koczan, K. Nomura, S. Y. He, Plant stomata function in innate
921 immunity against bacterial invasion. *Cell* **126**, 969–980 (2006).

922 78. X.-Y. Zheng, *et al.*, Spatial and temporal regulation of biosynthesis of the plant immune signal
923 salicylic acid. *Proc. Natl. Acad. Sci. U. S. A.* **112**, 9166–9173 (2015).

924 79. D. Goodspeed, E. W. Chehab, A. Min-Venditti, J. Braam, M. F. Covington, Arabidopsis
925 synchronizes jasmonate-mediated defense with insect circadian behavior. *Proc. Natl. Acad. Sci. U. S.*
926 *A.* **109**, 4674–4677 (2012).

927 80. I. S. Booij-James, W. M. Swegle, M. Edelman, A. K. Mattoo, Phosphorylation of the D1
928 photosystem II reaction center protein is controlled by an endogenous circadian rhythm. *Plant*
929 *Physiol.* **130**, 2069–2075 (2002).

930 81. A. N. Dodd, J. Kusakina, A. Hall, P. D. Gould, M. Hanaoka, The circadian regulation of
931 photosynthesis. *Photosynth. Res.* **119**, 181–190 (2014).

932 82. M. Edelman, A. K. Mattoo, D1-protein dynamics in photosystem II: the lingering enigma.
933 *Photosynth. Res.* **98**, 609–620 (2008).

934 83. D. L. Cano-Ramirez, *et al.*, Low-temperature and circadian signals are integrated by the sigma factor
935 SIG5. *Nat. Plants* **9**, 661–672 (2023).

936 84. Z. B. Noordally, *et al.*, Circadian control of chloroplast transcription by a nuclear-encoded timing
937 signal. *Science* **339**, 1316–1319 (2013).

938 85. L. Jouve, T. Gaspar, C. Kevers, H. Greppin, R. Degli Agosti, Involvement of indole-3-acetic acid in
939 the circadian growth of the first internode of Arabidopsis. *Planta* **209**, 136–142 (1999).

940 86. R. Rawat, *et al.*, REVEILLE1, a Myb-like transcription factor, integrates the circadian clock and
941 auxin pathways. *Proc. Natl. Acad. Sci. U. S. A.* **106**, 16883–16888 (2009).

942 87. B. A. McClure, G. Hagen, C. S. Brown, M. A. Gee, T. J. Guilfoyle, Transcription, organization, and
943 sequence of an auxin-regulated gene cluster in soybean. *Plant Cell* **1**, 229–239 (1989).

944 88. S. Ito, *et al.*, Genetic linkages between circadian clock-associated components and phytochrome-
945 dependent red light signal transduction in Arabidopsis thaliana. *Plant Cell Physiol.* **48**, 971–983
946 (2007).

947 89. K. A. Kaczorowski, P. H. Quail, Arabidopsis PSEUDO-RESPONSE REGULATOR7 is a signaling
948 intermediate in phytochrome-regulated seedling deetiolation and phasing of the circadian clock.
949 *Plant Cell* **15**, 2654–2665 (2003).

950 90. U. Hoecker, The activities of the E3 ubiquitin ligase COP1/SPA, a key repressor in light signaling.
951 *Curr. Opin. Plant Biol.* **37**, 63–69 (2017).

952 91. Y. Saijo, *et al.*, The COP1-SPA1 interaction defines a critical step in phytochrome A-mediated
953 regulation of HY5 activity. *Genes Dev.* **17**, 2642–2647 (2003).

954 92. Y. Yari Kamrani, *et al.*, Regulatory role of circadian clocks on ABA production and signaling,
955 stomatal responses, and water-use efficiency under water-deficit conditions. *Cells* **11**, 1154 (2022).

956 93. D. Seung, J. P. M. Risopatron, B. J. Jones, J. Marc, Circadian clock-dependent gating in ABA
957 signalling networks. *Protoplasma* **249**, 445–457 (2012).

958 94. T. Liu, J. Carlsson, T. Takeuchi, L. Newton, E. M. Farré, Direct regulation of abiotic responses by
959 the Arabidopsis circadian clock component PRR7. *Plant J.* **76**, 101–114 (2013).

960 95. Z. Wang, *et al.*, GAI functions in the plant response to dehydration stress in Arabidopsis thaliana.
961 *Int. J. Mol. Sci.* **21**, 819 (2020).

962 96. A. Fukushima, *et al.*, Impact of clock-associated Arabidopsis pseudo-response regulators in
963 metabolic coordination. *Proc. Natl. Acad. Sci. U. S. A.* **106**, 7251–7256 (2009).

964 97. N. Nakamichi, *et al.*, Transcript profiling of an Arabidopsis PSEUDO RESPONSE REGULATOR
965 arrhythmic triple mutant reveals a role for the circadian clock in cold stress response. *Plant Cell*
966 *Physiol.* **50**, 447–462 (2009).

967 98. S. J. Clough, A. F. Bent, Floral dip: a simplified method for*Agrobacterium*-mediated transformation
968 of*Arabidopsis thaliana*: Floral dip transformation of Arabidopsis. *Plant J.* **16**, 735–743 (1998).

969 99. P.-L. Germain, A. Lun, C. Garcia Meixide, W. Macnair, M. D. Robinson, Doublet identification in
970 single-cell sequencing data using scDblFinder. *F1000Res.* **10**, 979 (2021).

971 100. G. Wu, R. C. Anafi, M. E. Hughes, K. Kornacker, J. B. Hogenesch, MetaCycle: an integrated R
972 package to evaluate periodicity in large scale data. *Bioinformatics* **32**, 3351–3353 (2016).

973 101. J. R. Conway, A. Lex, N. Gehlenborg, UpSetR: an R package for the visualization of intersecting
974 sets and their properties. *Bioinformatics* **33**, 2938–2940 (2017).

975 102. V. A. Huynh-Thu, A. Irrthum, L. Wehenkel, P. Geurts, Inferring regulatory networks from
976 expression data using tree-based methods. *PLoS One* **5**, e12776 (2010).

977 103. S. Aibar, *et al.*, SCENIC: single-cell regulatory network inference and clustering. *Nat. Methods*
978 **14**, 1083–1086 (2017).

979 104. S. Cao, *et al.*, scPlant: A versatile framework for single-cell transcriptomic data analysis in plants.
980 *Plant Commun.* **4**, 100631 (2023).

981 105. P. Shannon, *et al.*, Cytoscape: a software environment for integrated models of biomolecular
982 interaction networks. *Genome Res.* **13**, 2498–2504 (2003).

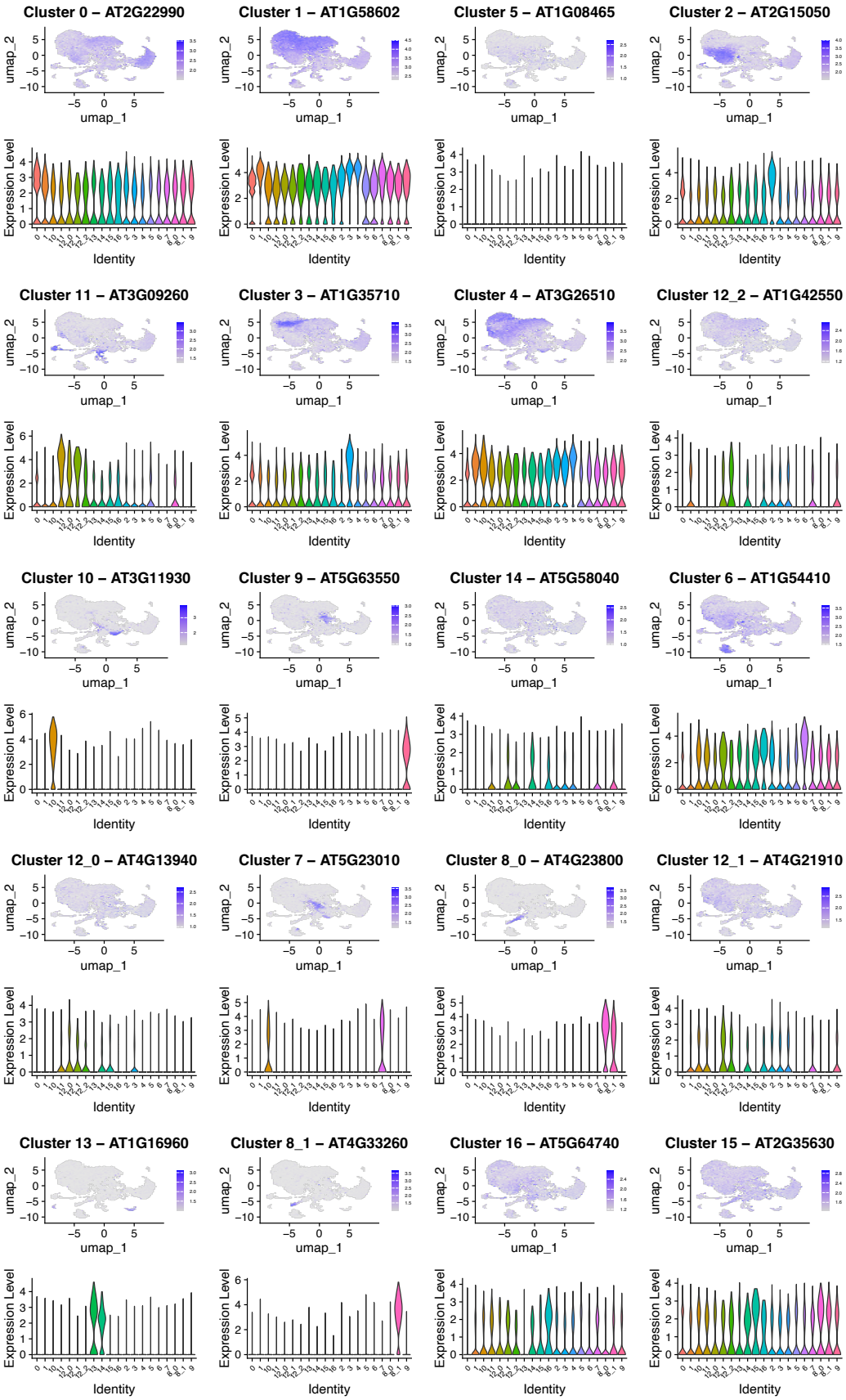
Cluster 0 – AT2G22990
Cluster 1 – AT1G58602
Cluster 5 – AT1G08465
Cluster 2 – AT2G15050
Cluster 11 – AT3G09260
Cluster 3 – AT1G35710
Cluster 4 – AT3G26510
Cluster 12_2 – AT1G42550
Cluster 10 – AT3G11930
Cluster 9 – AT5G63550
Cluster 14 – AT5G58040
Cluster 6 – AT1G54410
Cluster 12_0 – AT4G13940
Cluster 7 – AT5G23010
Cluster 8_0 – AT4G23800
Cluster 12_1 – AT4G21910
Cluster 13 – AT1G16960
Cluster 8_1 – AT4G33260
Cluster 16 – AT5G64740
Cluster 15 – AT2G35630
umap_1
umap_2
Expression Level
Identity

Figure S1. Top cluster biomarkers for all identified clusters. Expression feature plots (top) and cluster-based expression violin plots (bottom) for two genes with the highest average expression fold change between clusters.

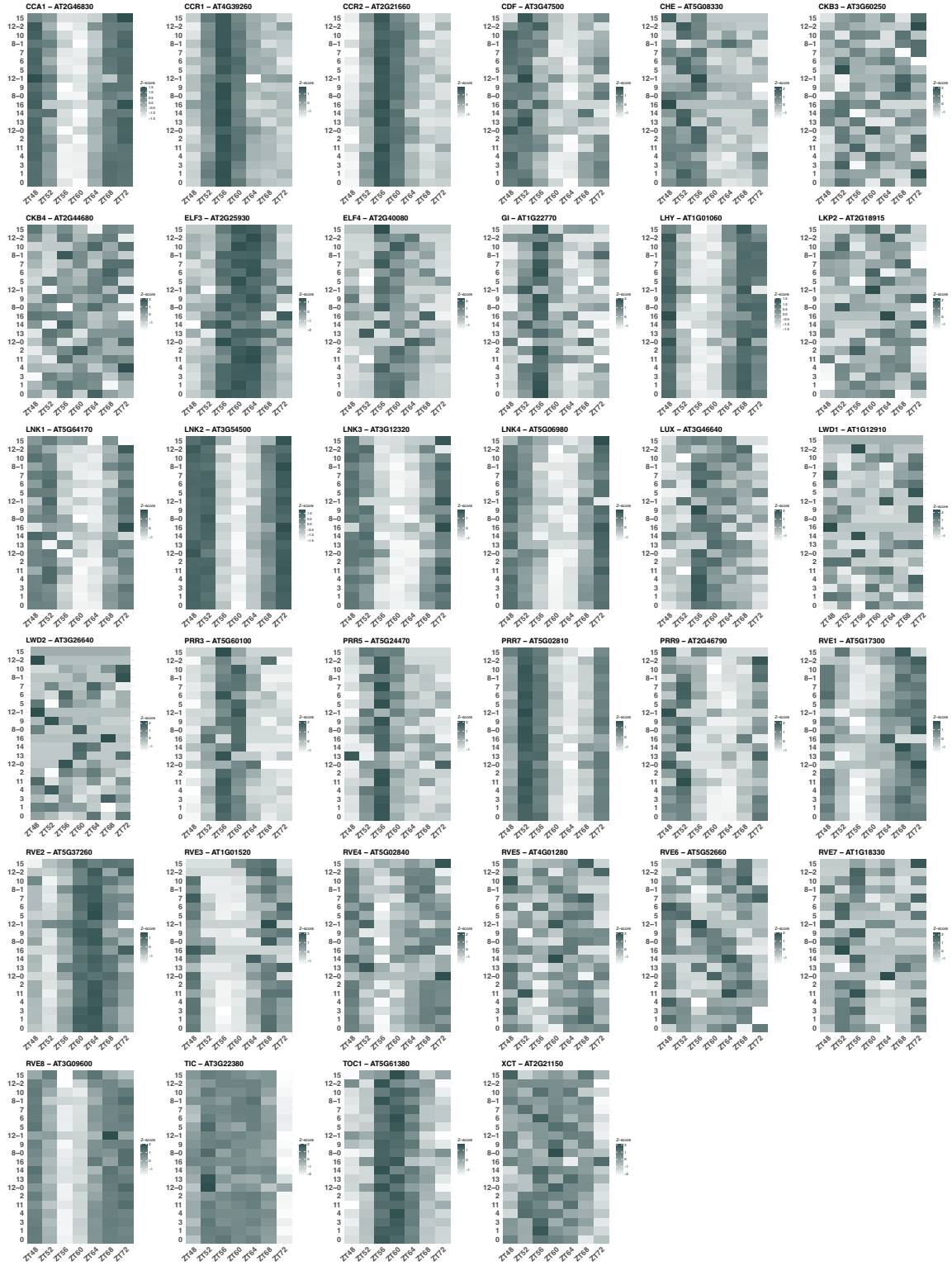

Fig S2. Cluster-resolved expression of key clock components and outputs. Expression is plotted as a Z-score over a circadian day, as in Fig 2B.

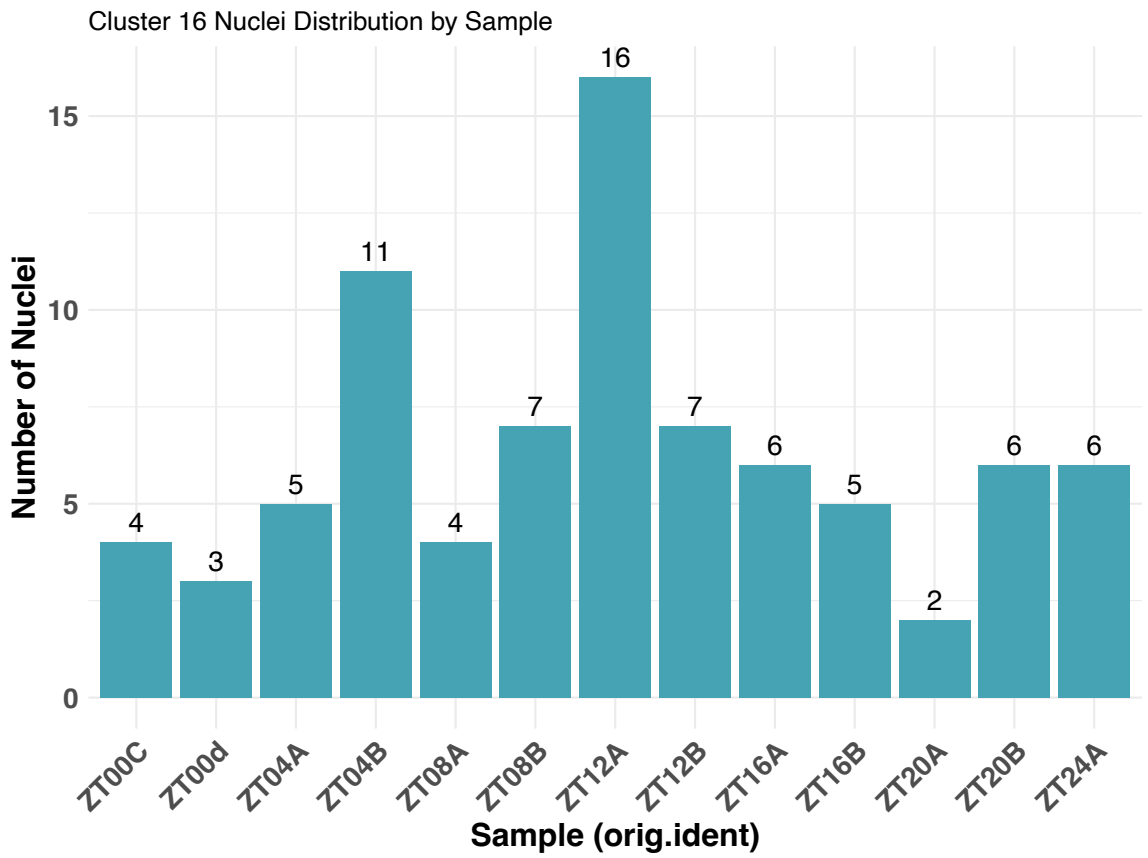

Fig S3. Distribution of root hair cells inadvertently captured across each library. These cell types were not specifically targeted during collection and are expected in low abundance.

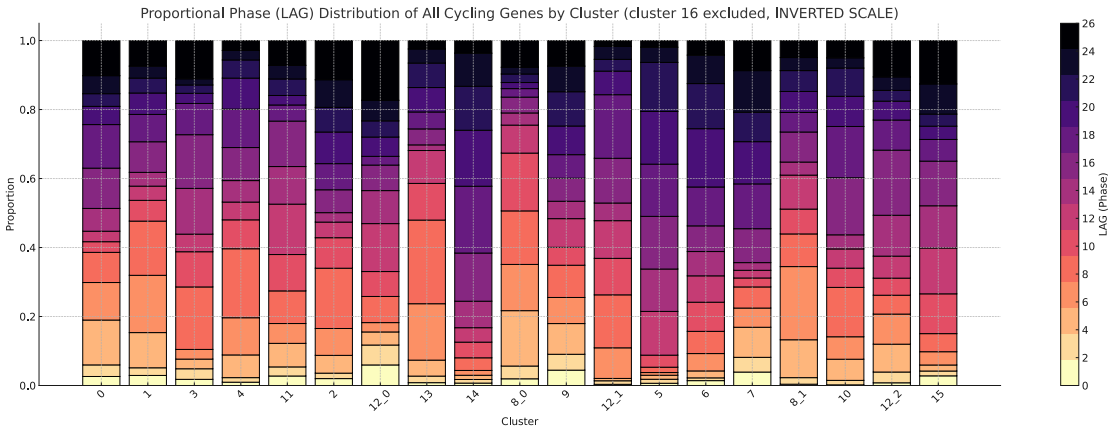

Fig S4. Distribution of peak expression for cycling genes in each cluster. LAG represents peak expression or phase across the circadian day, as determined through CycleJTK.

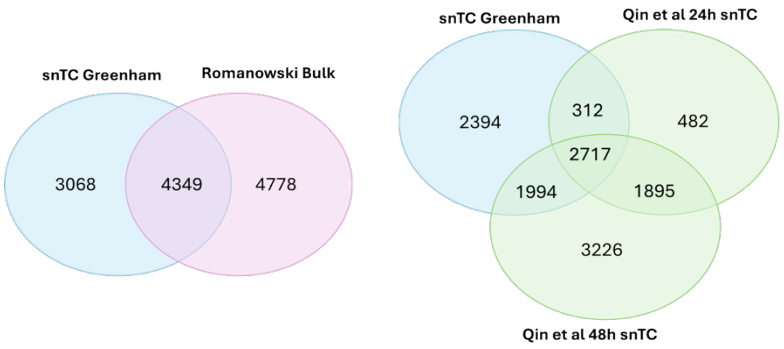

Fig S5. Overlap in cycling gene identification across studies. (A) Overlap of the cluster based cycling genes in our study with genes identified as cycling in Romanowski et al. (B) Overlap of cluster-resolved cycling genes in our study with genes identified as cycling in both the 24- and 48-hour Qin et al datasets.

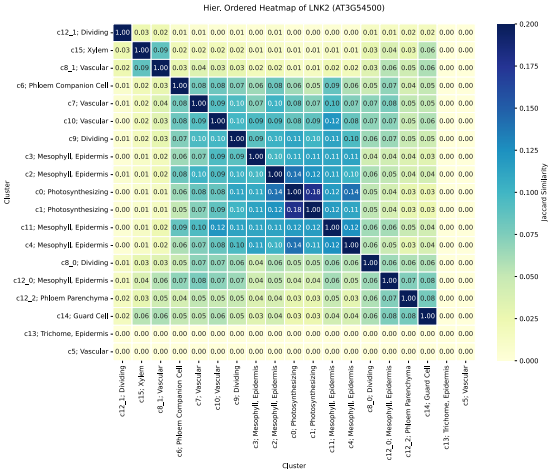
Hier. Ordered Heatmap of LNK2 (AT3G54500)
Cluster
Jaccard Similarity

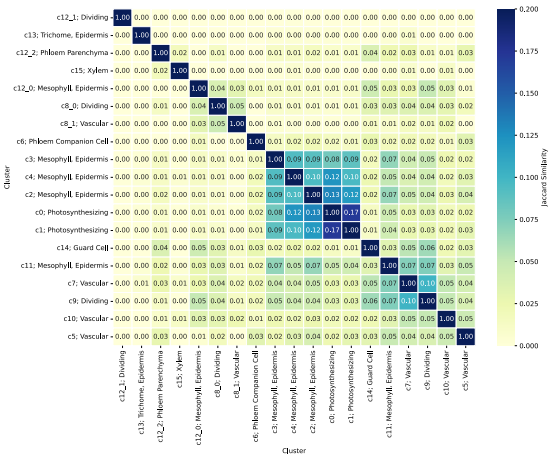
Hier. Ordered Heatmap of PRR7 (AT5G02810)
Cluster
Jaccard Similarity

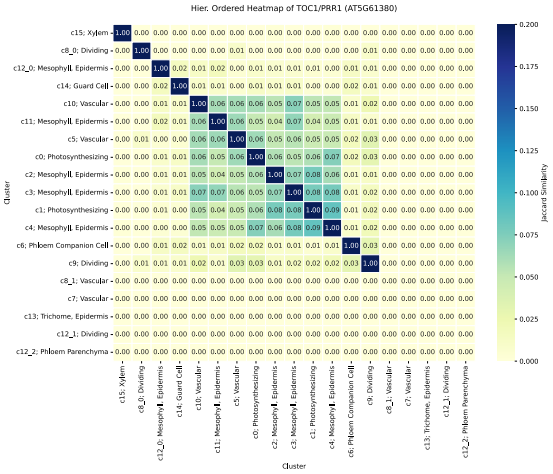
Hier. Ordered Heatmap of TOC1/PRR1 (AT5G61380)
Cluster
Jaccard Similarity

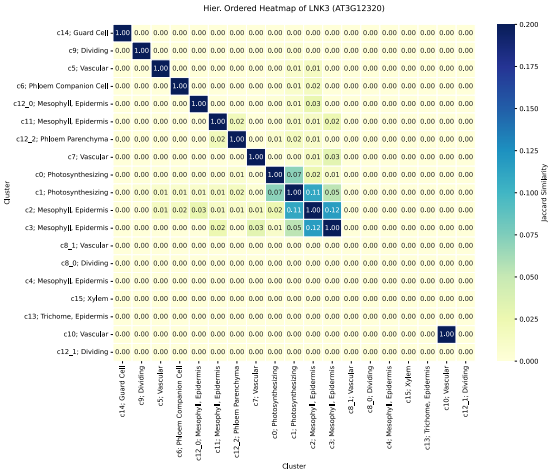
Hier. Ordered Heatmap of LNK3 (AT3G12320)
Cluster
Jaccard Similarity

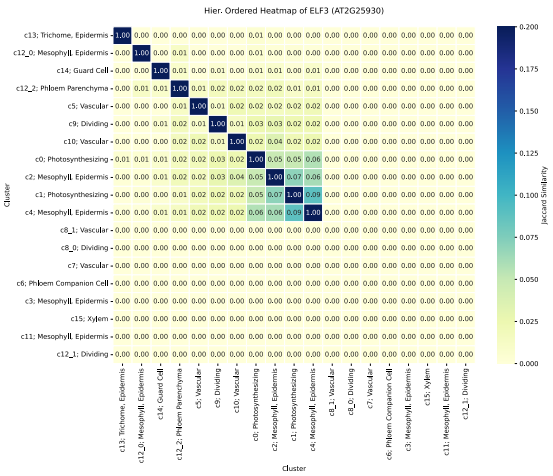
Hier. Ordered Heatmap of ELF3 (AT2G25930)
Cluster
Jaccard Similarity

Fig S6. Jaccard similarity indices for several circadian clock component centered scGRNs. Similarity indices were calculated between all pairs of cluster specific scGRNs for LNK2, PRR7, TOC1, LNK3, and ELF3, with darker blue indicating more similar scGRNs.

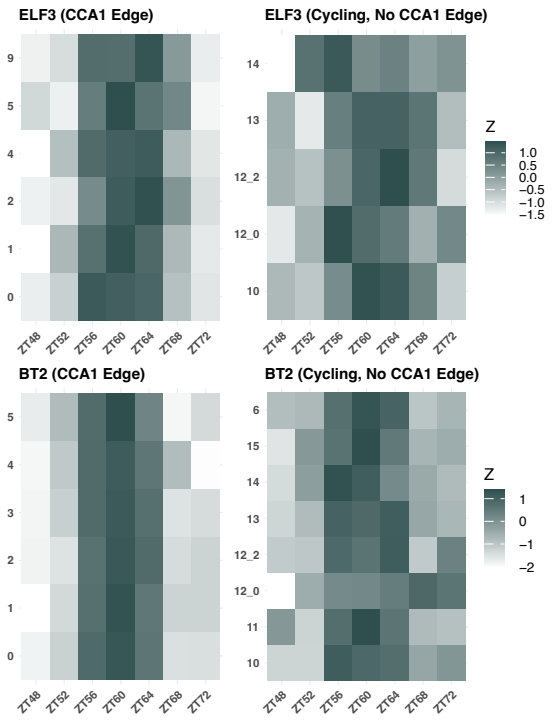

Fig S7. Cluster-resolved expression for genes identified as *CCA1* targets through scGRN prediction and supported by previously published ChIP-seq binding data. Cluster-resolved circadian expression patterns for ELF3 and BT2, split by presence or absence of a scGRN-derived CCA1 edge.